FERMILAB-Pub-00/334-T
SCIPP-01/25
UCD-01-23
hep-ph/0106116

Distinguishing a MSSM Higgs Boson from the SM Higgs Boson at a Linear Collider

Marcela Carena[a], Howard E. Haber[b], Heather E. Logan[a] and Stephen Mrenna[c] *

[a] *Theoretical Physics Department*
Fermi National Accelerator Laboratory, Batavia, IL 60510-0500, USA.
[b] *Santa Cruz Institute for Particle Physics*
University of California, Santa Cruz, CA 95064, USA.
[c] *Davis Institute for High Energy Physics*
University of California, Davis, CA 95616, USA.

Abstract

The decoupling properties of the Higgs sector in the Minimal Supersymmetric Standard Model (MSSM) imply that a light CP-even Higgs boson discovered at the Tevatron or LHC may closely resemble the Standard Model (SM) Higgs boson. In this paper, we investigate how precision measurements of Higgs properties at a Linear Collider (LC) can distinguish between a CP-even Higgs boson of the MSSM and the SM Higgs boson. We review the expected theoretical behavior of the partial widths and branching ratios for decays of the neutral MSSM Higgs bosons with significant couplings to the W and Z bosons, including the leading radiative corrections to the mixing angle α and $\tan\beta$-enhanced vertex corrections. The general expectation is that the Higgs couplings to W^+W^-, ZZ, $c\bar{c}$ and $t\bar{t}$ should quickly approach their SM values for increasing CP-odd Higgs mass m_A, while the couplings to $b\bar{b}$ and $\tau^+\tau^-$ do so more slowly. Using the expected experimental and theoretical accuracy in determining SM branching ratios and partial widths, we demonstrate the sensitivity of measurements at the LC to variations in the MSSM parameters, with particular attention to the decoupling limit. For a wide range of MSSM parameters, the LC is sensitive to $m_A \sim 600$ GeV almost independently of $\tan\beta$. For large values of $\tan\beta$ and some specific choices of MSSM parameters [*e.g.*, $A_t\mu < 0$ and $|A_t| \simeq |\mu| \simeq \mathcal{O}(M_S)$], one of the CP-even Higgs bosons can be SM-like independent of the value of m_A. In the case of large deviations from the SM, we present a procedure using Higgs coupling measurements to extract the supersymmetric correction to the relation between the b quark mass and Yukawa coupling.

*Electronic addresses: carena@fnal.gov, haber@scipp.ucsc.edu, logan@fnal.gov, mrenna@physics.ucdavis.edu

1 Introduction

The radiative corrections to Higgs boson masses and couplings in the minimal supersymmetric extension of the Standard Model (MSSM) have been investigated thoroughly using different theoretical approaches. Derived quantities such as Higgs boson production cross sections, partial widths and branching ratios (BRs) are predicted to a high level of precision for any given set of MSSM parameters. While at least one of the neutral Higgs bosons of the MSSM has a coupling to W and Z bosons similar in magnitude to a Standard Model (SM) Higgs boson, some of its properties can differ from those of the SM Higgs boson of the same mass. Nevertheless, over a significant region of parameter space, the deviation of the couplings of this SM-like[1] Higgs boson from the corresponding couplings of the SM Higgs boson is small and approaches zero in the so-called "decoupling limit" of the model [1].

Experiments at the Fermilab Tevatron [2] and CERN LHC [3] will be sensitive to the Higgs bosons of the SM and MSSM. The Tevatron can discover a SM-like Higgs boson for most choices of MSSM parameters if enough data can be accumulated, the detectors perform as expected, and systematic errors are demonstrably small. The LHC can discover at least one MSSM Higgs boson over all of the MSSM parameter space [3], and several Higgs bosons are likely to be discovered in a significant region of the parameter space. For moderate values of the ratio, $\tan\beta$, of the two Higgs vacuum expectation values,[2] in the range $2.4 \lesssim \tan\beta \lesssim 8$ [$2.4 \lesssim \tan\beta \lesssim 17$] for a CP-odd Higgs mass of $m_A = 250$ GeV [$m_A = 500$ GeV], only one SM-like Higgs boson will be visible at the LHC [3, 5]. If more than one Higgs boson is observed at the hadron colliders, then additional precision measurements of Higgs decay properties can determine if the Higgs bosons originate from a two-Higgs doublet sector of a supersymmetric (SUSY) model (as in the MSSM) or from a different model. If only one Higgs boson is observed, such precision measurements could indicate whether any additional Higgs structure exists. Of course, the MSSM also contains supersymmetric particles, which can be discovered at the Tevatron and/or the LHC. However, these particles can be heavy, so that only a part of the spectrum may ultimately be observable at the LHC, or the interpretation of the data as SUSY particle production may be ambiguous. Hence, precision measurements of the properties of the Higgs sector can provide crucial supporting evidence for the MSSM. In this study, we explore the potential of a future e^+e^- linear collider (LC) to explore the MSSM Higgs sector in regions of MSSM parameter space with very different behaviors.

If a Higgs boson couples to Z bosons with SM-like strength, then its mass can be determined to high precision at the LC through measurements of the recoil mass spectrum against a Z boson. With 500 fb^{-1}

[1] In this paper, a SM-like Higgs boson always refers to the neutral Higgs boson of the MSSM with $g^2_{h_i VV} \geq 0.5 g^2_{h_{\rm SM} VV}$, where $V = W$ or Z. The decay properties of this Higgs boson may be quite different than those of a SM Higgs boson in the parameter regime away from the decoupling limit.

[2] The absence of a Higgs boson discovery at LEP implies that the range $0.5 < \tan\beta < 2.4$ is excluded at 95% confidence level [4].

of data at $\sqrt{s} = 350$ GeV, a precision of 40–90 MeV can be achieved for Higgs masses between 120 and 180 GeV [6, 7]. With the mass of the Higgs boson so constrained, the theoretical predictions for many of the Higgs branching ratios and partial widths (*i.e.*, the Higgs couplings) will be known to great accuracy. As a result, precision experimental measurements of Higgs branching ratios and partial widths may allow one to discriminate between the SM and new physics of electroweak symmetry breaking. A number of recent studies have evaluated how precisely the branching ratios and couplings of the SM Higgs boson can be measured at the LC [7–13]. In this paper, we exploit the results of these studies to examine the potential of Higgs boson BR and partial width measurements at the LC to distinguish the SM-like Higgs boson of the MSSM from the SM Higgs boson. We focus on choices of MSSM parameters that exhibit a significant variation in the approach to the decoupling limit. This allows us to identify parameter regions where hadron collider measurements will most likely not be able to distinguish a MSSM from the SM Higgs boson, and LC measurements can be essential for this purpose. In addition, one new observation is that there are regions where decoupling occurs at fairly low values of m_A so that precision measurements will not be able to reveal much about the MSSM parameter space structure. In such cases, direct measurements of the properties of the heavier Higgs bosons will be necessary to elucidate the true nature of the Higgs sector. Even if the existence of a MSSM Higgs boson is established, it may be challenging to extract the underlying MSSM parameters [14]. Nevertheless, in some regions of MSSM parameter space, we demonstrate that the SUSY vertex corrections to the Higgs boson couplings to bottom quark and tau pairs can be extracted from branching ratio and Higgs coupling measurements.[3]

This paper is organized as follows. In Sec. 2, we outline the features of the MSSM Higgs sector relevant for our analysis. In particular, we review and expand on the details of the radiative corrections that contribute significantly to the Higgs couplings. In Sec. 3, we analyze the behavior of the Higgs partial decay widths in various regions of MSSM parameter space. We consider three benchmark scenarios that lead to very different behaviors in the MSSM Higgs sector. In Sec. 4, we combine the expected experimental capabilities of the LC to measure Higgs boson BRs and couplings with our theoretical results. For the benchmark scenarios, we quantify the ability of the LC to distinguish the lightest MSSM Higgs boson from the SM Higgs boson. In Sec. 5, we describe how the SUSY Yukawa correction to the Higgs boson couplings to bottom quark pairs, Δ_b, can be extracted from Higgs measurements. In Sec. 4 and 5 we also evaluate the impact of the theoretical uncertainties on our analysis. Finally, Sec. 6 contains our conclusions. Some preliminary results of this work were presented in Ref. [17].

[3]The distinctive effects of SUSY vertex corrections to Higgs-fermion pair couplings on branching ratio measurements have also been explored in Refs. [15, 16].

2 The MSSM Higgs sector

In this section, we review those properties of the MSSM Higgs sector relevant to our analysis. At tree level, the masses and couplings of the MSSM Higgs bosons are determined by two parameters, which are conveniently chosen to be the mass of the CP-odd Higgs boson, m_A, and the ratio of the vacuum expectation values of the two neutral Higgs fields, $\tan\beta$. Radiative corrections to the MSSM Higgs sector introduce significant dependence on other MSSM parameters (for a review see Ref. [2]). These radiative corrections have been analyzed extensively in the literature [2, 18–45].

The two main sources of radiative corrections to the couplings of the MSSM Higgs bosons are: (i) the radiative corrections to the Higgs squared-mass matrix [18–38], which give rise to corrections to an effective CP-even Higgs mixing angle α, and (ii) vertex corrections to the Higgs-fermion Yukawa couplings [27,39–45]. In this paper we examine the effects of these two types of corrections in the CP-conserving MSSM.[4]

The squared-mass matrix for the CP-even neutral MSSM Higgs bosons h and H (where $m_h < m_H$) is given by:

$$\mathcal{M}^2 \equiv \begin{pmatrix} \mathcal{M}^2_{11} & \mathcal{M}^2_{12} \\ \mathcal{M}^2_{12} & \mathcal{M}^2_{22} \end{pmatrix} = \begin{pmatrix} m_A^2 s_\beta^2 + m_Z^2 c_\beta^2 & -(m_A^2 + m_Z^2) s_\beta c_\beta \\ -(m_A^2 + m_Z^2) s_\beta c_\beta & m_A^2 c_\beta^2 + m_Z^2 s_\beta^2 \end{pmatrix} + \delta\mathcal{M}^2 \,, \tag{2.1}$$

where $\delta\mathcal{M}^2$ is a consequence of the radiative corrections. At tree level, one obtains $m_h \leq m_Z |\cos 2\beta| \leq m_Z$. Such a light h is essentially ruled out by searches at LEP2.[5] However, once radiative corrections to the squared-mass matrix are included, the theoretical upper bound on m_h is raised substantially. For a fixed value of $\tan\beta$ and a specified set of MSSM parameters, m_h grows with increasing m_A and reaches an asymptotic value $m_h^{\max}(\tan\beta)$ in the limit of large m_A. If $\tan\beta$ is now allowed to vary (while holding all other free parameters fixed), $m_h^{\max}(\tan\beta)$ increases with $\tan\beta$ and typically[6] reaches an asymptotic value $m_h^{\max}$ for $\tan\beta \gtrsim 10$. For large values of $\tan\beta$, $m_h \simeq m_h^{\max}$ and $m_H \simeq m_A$ for $m_A > m_h^{\max}$. Conversely, if $m_A < m_h^{\max}$ then $m_h \simeq m_A$ and $m_H \simeq m_h^{\max}$.

At the LC, a light SM-like Higgs boson will be produced through Higgsstrahlung [$e^+e^- \to Z^* \to Zh$], WW fusion [$e^+e^- \to W^*W^*\nu\bar{\nu} \to h\nu\bar{\nu}$] and ZZ fusion [$e^+e^- \to Z^*Z^*e^+e^- \to he^+e^-$]. The cross sections for all the above processes depend on the couplings of the Higgs boson to vector boson pairs. In the MSSM, the couplings of h [H] to vector boson pairs are given by $\sin(\beta-\alpha)$ [$\cos(\beta-\alpha)$] times the corresponding SM Higgs coupling. The decoupling limit corresponds to $m_A \gg m_Z$, in which case $\sin(\beta-\alpha) \simeq 1$, and the properties of h approach those of the SM Higgs boson. The CP-even Higgs squared-masses obey the sum

[4] The MSSM Higgs sector automatically conserves CP at tree-level, although non-trivial CP-violating effects can enter at one-loop (due to complex MSSM parameters) and be phenomenologically significant [46, 47]. In this paper, we assume that the one-loop CP-violating effects are absent. The CP-violating case will be addressed elsewhere.

[5] The current MSSM Higgs mass limits are $m_h > 91.0$ GeV and $m_A > 91.9$ GeV [4].

[6] In some regions of MSSM parameter space at large $\tan\beta$, radiative corrections to the Higgs-bottom quark Yukawa coupling can yield large negative loop corrections to $m_h^{\max}(\tan\beta)$, so that the latter begins to decrease for $\tan\beta \gtrsim 10$.

rule [48, 49]

$$m_H^2 \cos^2(\beta-\alpha) + m_h^2 \sin^2(\beta-\alpha) = \left[m_h^{\rm max}(\tan\beta)\right]^2 . \tag{2.2}$$

In particular, combining this sum rule with the large $\tan\beta$ behavior of the Higgs masses noted above implies that H is the SM-like Higgs boson for $m_A < m_h^{\rm max}$ and large values of $\tan\beta$, while h is the SM-like Higgs boson for $m_A > m_h^{\rm max}$. Note that the decoupling limit implies that the latter holds for any value of $\tan\beta$. Most of the analysis of this paper will focus on the case where h is the SM-like Higgs boson and $m_A > m_h^{\rm max}$.

Along with $\tan\beta$, the CP-even Higgs mixing angle α determines the Higgs boson couplings to fermions. In particular, relative to their SM values, the couplings of h [H] to down-type fermions are multiplied by $-\sin\alpha/\cos\beta$ [$\cos\alpha/\cos\beta$], and those of h [H] to up-type fermions are multiplied by $\cos\alpha/\sin\beta$ [$\sin\alpha/\sin\beta$]. Thus radiative corrections to α can have significant effects on the Higgs boson couplings to fermions. The mixing angle α which diagonalizes the mass matrix in Eq. 2.1 can be expressed as:

$$s_\alpha c_\alpha = \frac{\mathcal{M}_{12}^2}{\sqrt{({\rm Tr}\mathcal{M}^2)^2 - 4\,{\rm det}\mathcal{M}^2}}\,, \qquad c_\alpha^2 - s_\alpha^2 = \frac{\mathcal{M}_{11}^2 - \mathcal{M}_{22}^2}{\sqrt{({\rm Tr}\mathcal{M}^2)^2 - 4\,{\rm det}\mathcal{M}^2}}\,, \tag{2.3}$$

where $s_\alpha \equiv \sin\alpha$ and $c_\alpha \equiv \cos\alpha$. Note that if $\mathcal{M}_{12}^2 \to 0$, then either $\sin\alpha \to 0$ (if $\mathcal{M}_{11}^2 > \mathcal{M}_{22}^2$) or $\cos\alpha \to 0$ (if $\mathcal{M}_{11}^2 < \mathcal{M}_{22}^2$). At tree level (see Eq. 2.1), $\mathcal{M}_{12}^2$ is small for small m_A and/or large $\tan\beta$, but it cannot vanish. This is no longer true after including radiative corrections, which can be of the same order as the tree level value for small values of m_A and large $\tan\beta$. In particular, the radiatively-corrected value of $\mathcal{M}_{12}^2$ exhibits a widely varying behavior as a function of the MSSM parameters. The radiative corrections to $\mathcal{M}^2$, including dominant corrections coming from the one-loop top and bottom quark and top and bottom squark contributions plus the two-loop leading logarithmic contributions, are given to $\mathcal{O}(h_t^4, h_b^4)$ by [29, 43]

$$\begin{aligned}
\delta\mathcal{M}_{11}^2 &\simeq -\bar{\mu}^2 x_t^2 \frac{h_t^4 v^2}{32\pi^2} s_\beta^2 \left[1 + c_{11}\ln\left(\frac{M_S^2}{m_t^2}\right)\right] - \bar{\mu}^2 a_b^2 \frac{h_b^4 v^2}{32\pi^2} s_\beta^2 \left[1 + c_{12}\ln\left(\frac{M_S^2}{m_t^2}\right)\right], \\
\delta\mathcal{M}_{22}^2 &\simeq \frac{3h_t^4 v^2}{8\pi^2} s_\beta^2 \ln\left(\frac{M_S^2}{m_t^2}\right)\left[1 + \tfrac{1}{2}c_{21}\ln\left(\frac{M_S^2}{m_t^2}\right)\right] \\
&\quad + \frac{h_t^4 v^2}{32\pi^2} s_\beta^2 x_t a_t (12 - x_t a_t)\left[1 + c_{21}\ln\left(\frac{M_S^2}{m_t^2}\right)\right] - \bar{\mu}^4 \frac{h_b^4 v^2}{32\pi^2} s_\beta^2 \left[1 + c_{22}\ln\left(\frac{M_S^2}{m_t^2}\right)\right], \\
\delta\mathcal{M}_{12}^2 &\simeq -\bar{\mu} x_t \frac{h_t^4 v^2}{32\pi^2}(6 - x_t a_t) s_\beta^2 \left[1 + c_{31}\ln\left(\frac{M_S^2}{m_t^2}\right)\right] + \bar{\mu}^3 a_b \frac{h_b^4 v^2}{32\pi^2} s_\beta^2 \left[1 + c_{32}\ln\left(\frac{M_S^2}{m_t^2}\right)\right],
\end{aligned} \tag{2.4}$$

where $s_\beta \equiv \sin\beta$, $c_\beta \equiv \cos\beta$, and the coefficients c_{ij} are:

$$c_{ij} \equiv \frac{t_{ij} h_t^2 + b_{ij} h_b^2 - 32 g_3^2}{32\pi^2}\,, \tag{2.5}$$

with $(t_{11}, t_{12}, t_{21}, t_{22}, t_{31}, t_{32}) = (12, -4, 6, -10, 9, -7)$ and $(b_{11}, b_{12}, b_{21}, b_{22}, b_{31}, b_{32}) = (-4, 12, 2, 18, -1, 15)$. Above, h_t and h_b are the top and bottom quark Yukawa couplings [see Eqs. 2.6–2.8], g_3 is the strong QCD

coupling, $v = 246$ GeV is the SM Higgs vacuum expectation value, and $M_S^2 = \frac{1}{2}(M_{\tilde{t}_1}^2 + M_{\tilde{t}_2}^2)$ is the average squared top squark mass.[7] The $\delta\mathcal{M}_{ij}^2$ also depend on the MSSM parameters A_t, A_b and μ that enter the off-diagonal top-squark and bottom-squark squared-mass matrices. We employ the following notation: $\bar{\mu} \equiv \mu/M_S$, $a_t \equiv A_t/M_S$, $a_b \equiv A_b/M_S$ and $x_t \equiv X_t/M_S$, where $X_t \equiv A_t - \mu\cot\beta$. Note that the leading radiative corrections to $\mathcal{M}_{12}^2$ depend strongly on the sign of μX_t and the magnitude of A_t. For the scenarios we shall consider, with $a_t^2 \lesssim 6$, the combination $A_t\mu < 0$ [$A_t\mu > 0$] can lead to a suppression [enhancement] of $\mathcal{M}_{12}^2 = -(m_A^2 + m_Z^2)s_\beta c_\beta + \delta\mathcal{M}_{12}^2$, and hence, to a suppression [enhancement] of the coupling of the SM-like Higgs boson to b quarks and τ leptons.

Our numerical calculation of the radiative corrections to the Higgs masses and mixing angle is based on the results of Ref. [36] and incorporates the renormalization group improved one-loop effective potential, plus the non-logarithmic two-loop contributions of the Yukawa vertex corrections for top and bottom quarks. The Yukawa vertex corrections modify the effective Lagrangian that describes the coupling of the Higgs bosons to the third generation quarks:[8]

$$-\mathcal{L}_{\rm eff} = \epsilon_{ij}\left[(h_b + \delta h_b)\bar{b}_R H_d^i Q_L^j + (h_t + \delta h_t)\bar{t}_R Q_L^i H_u^j\right] + \Delta h_t \bar{t}_R Q_L^k H_d^{k*} + \Delta h_b \bar{b}_R Q_L^k H_u^{k*} + \text{h.c.}\,, \qquad (2.6)$$

resulting in a modification of the tree-level relation between h_t [h_b] and m_t [m_b] as follows:

$$m_b = \frac{h_b v}{\sqrt{2}}\cos\beta\left(1 + \frac{\delta h_b}{h_b} + \frac{\Delta h_b \tan\beta}{h_b}\right) \equiv \frac{h_b v}{\sqrt{2}}\cos\beta(1+\Delta_b)\,, \qquad (2.7)$$

$$m_t = \frac{h_t v}{\sqrt{2}}\sin\beta\left(1 + \frac{\delta h_t}{h_t} + \frac{\Delta h_t \cot\beta}{h_t}\right) \equiv \frac{h_t v}{\sqrt{2}}\sin\beta(1+\Delta_t)\,. \qquad (2.8)$$

The dominant contributions to Δ_b are $\tan\beta$-enhanced, with $\Delta_b \simeq (\Delta h_b/h_b)\tan\beta$; for $\tan\beta \gg 1$, $\delta h_b/h_b$ provides a small correction to Δ_b. In the same limit, $\Delta_t \simeq \delta h_t/h_t$, with the additional contribution of $(\Delta h_t/h_t)\cot\beta$ providing a small correction.[9] Explicitly, one finds that for $\tan\beta \gg 1$ [27, 40, 41]

$$\Delta_b \simeq \left[\frac{2\alpha_s}{3\pi}\mu M_{\tilde{g}}\, I(M_{\tilde{b}_1}^2, M_{\tilde{b}_2}^2, M_{\tilde{g}}^2) + \frac{h_t^2}{16\pi^2}\mu A_t\, I(M_{\tilde{t}_1}^2, M_{\tilde{t}_2}^2, \mu^2)\right]\tan\beta\,, \qquad (2.9)$$

$$\Delta_t \simeq -\frac{2\alpha_s}{3\pi}A_t M_{\tilde{g}} I(M_{\tilde{t}_1}^2, M_{\tilde{t}_2}^2, M_{\tilde{g}}^2) - \frac{h_b^2}{16\pi^2}\mu^2 I(M_{\tilde{b}_1}^2, M_{\tilde{b}_2}^2, \mu^2), \qquad (2.10)$$

where $\alpha_s \equiv g_3^2/4\pi$, $M_{\tilde{g}}$ is the gluino mass, $M_{\tilde{b}_{1,2}}$ are the bottom squark masses, and smaller electroweak corrections have been ignored. The loop integral $I(a^2, b^2, c^2)$ is of order $1/\max(a^2, b^2, c^2)$ when at least one of its arguments is large compared to m_Z^2; for the explicit expression see Ref. [41]. These one-loop Yukawa

[7] Eq. 2.4 is derived under the assumption that $|M_{\tilde{t}_1}^2 - M_{\tilde{t}_2}^2|/(M_{\tilde{t}_1}^2 + M_{\tilde{t}_2}^2) \ll 1$. The approximate forms of Eq. 2.4 are sufficient to provide insight on the dependence of the radiatively-corrected Higgs masses and couplings on the MSSM parameters. The numerical work of this paper employs more exact expressions for the Higgs squared-mass matrix elements as noted below.

[8] The Higgs couplings to leptons and to first and second generation quarks can be treated similarly.

[9] Because the one-loop corrections δh_b, Δh_b, δh_t and Δh_t depend only on Yukawa and gauge couplings and SUSY particle masses, they contain no hidden $\tan\beta$ enhancements [50].

vertex corrections enter indirectly as two-loop effects in the Higgs squared-mass matrix elements via the dependence on h_t and h_b.

We have noted earlier that in the decoupling limit $\sin(\beta-\alpha)=1$ [or equivalently $\cos(\beta-\alpha)=0$], in which case the couplings of h are identical to those of the SM Higgs boson. This limit is achieved when $m_A \gg m_Z$. This behavior, which is easy to verify for the tree-level expressions, continues to hold when radiative corrections are included. However, the onset of decoupling can be significantly affected by the radiative corrections, as we now discuss. From Eq. 2.3, one easily obtains:

$$\begin{aligned}\cos(\beta-\alpha) &= \frac{(\mathcal{M}_{11}^2-\mathcal{M}_{22}^2)\sin 2\beta - 2\mathcal{M}_{12}^2\cos 2\beta}{2(m_H^2-m_h^2)\sin(\beta-\alpha)} \\ &= \frac{m_Z^2\sin 4\beta + (\delta\mathcal{M}_{11}^2-\delta\mathcal{M}_{22}^2)\sin 2\beta - 2\delta\mathcal{M}_{12}^2\cos 2\beta}{2(m_H^2-m_h^2)\sin(\beta-\alpha)\,.}\end{aligned} \tag{2.11}$$

Since $\delta\mathcal{M}_{ij}^2 \sim \mathcal{O}(m_Z^2)$, and $m_H^2-m_h^2 = m_A^2+\mathcal{O}(m_Z^2)$, one obtains for $m_A \gg m_Z$

$$\cos(\beta-\alpha) = c\left[\frac{m_Z^2\sin 4\beta}{2m_A^2} + \mathcal{O}\left(\frac{m_Z^4}{m_A^4}\right)\right], \tag{2.12}$$

where

$$c \equiv 1 + \frac{\delta\mathcal{M}_{11}^2-\delta\mathcal{M}_{22}^2}{2m_Z^2\cos 2\beta} - \frac{\delta\mathcal{M}_{12}^2}{m_Z^2\sin 2\beta}\,. \tag{2.13}$$

Eq. 2.12 exhibits the expected decoupling behavior for $m_A \gg m_Z$. However, Eq. 2.11 exhibits another way in which $\cos(\beta-\alpha)=0$ can be achieved—simply choose the supersymmetric parameters (that govern the Higgs mass radiative corrections) such that the numerator of Eq. 2.11 vanishes. That is,[10]

$$2m_Z^2\sin 2\beta = 2\,\delta\mathcal{M}_{12}^2 - \tan 2\beta\left(\delta\mathcal{M}_{11}^2-\delta\mathcal{M}_{22}^2\right). \tag{2.14}$$

Note that Eq. 2.14 is independent of the value of m_A. For a typical choice of MSSM parameters, Eq. 2.14 yields a solution at large $\tan\beta$—by approximating $\tan 2\beta \simeq -\sin 2\beta \simeq -2/\tan\beta$, one can determine the value of β at which the decoupling occurs:

$$\tan\beta \simeq \frac{2m_Z^2-\delta\mathcal{M}_{11}^2+\delta\mathcal{M}_{22}^2}{\delta\mathcal{M}_{12}^2}\,. \tag{2.15}$$

The explicit expressions for $\delta\mathcal{M}_{ij}^2$ quoted in Eq. 2.4 confirm that the assumption of $\tan\beta \gg 1$ used to derive this result is a consistent approximation because $\delta\mathcal{M}_{12}^2$ is typically small. We conclude that for the value of $\tan\beta$ specified in Eq. 2.15, $\cos(\beta-\alpha)=0$ independently of the value of m_A. We shall refer to this phenomenon as m_A-independent decoupling. From Eq. 2.4, it follows that explicit solutions to Eq. 2.14 depend on ratios of SUSY parameters and so are insensitive to the overall SUSY mass scale, modulo a mild logarithmic dependence on M_S/m_t.

[10] Eq. 2.14 is equivalent to the condition $c=0$ [see Eqs. 2.12 and 2.13].

The introduction of the radiatively-corrected value for the CP-even Higgs mixing angle α affects the MSSM Higgs boson couplings to all down-type fermions (and likewise to all up-type fermions) in the same way. In particular,[11] $\mathrm{BR}(b)/\mathrm{BR}(\tau) = \Gamma(b)/\Gamma(\tau) \propto g^2_{hbb}/g^2_{h\tau\tau} \propto m_b^2/m_\tau^2$ [15,16,43,51]. However, the Yukawa vertex corrections enter directly in the couplings of fermions to the Higgs bosons. These corrections can be understood as a modification of the relation between the fermion Yukawa coupling and its mass, as exhibited in Eqs. 2.7–2.8. After including the dominant corrections, the CP-even Higgs boson couplings to b and τ are modified relative to the SM coupling, $g_{h_{\rm SM}ff} = gm_f/2m_W$, as follows [43]:

$$\begin{aligned} g_{hbb} &= -\frac{gm_b\sin\alpha}{2m_W\cos\beta}\,\frac{1}{1+\Delta_b}\left[1-\Delta_b\cot\alpha\cot\beta+\frac{\delta h_b}{h_b}\,(1+\cot\alpha\cot\beta)\right], \\ g_{Hbb} &= \frac{gm_b\cos\alpha}{2m_W\cos\beta}\,\frac{1}{1+\Delta_b}\left[1+\Delta_b\tan\alpha\cot\beta+\frac{\delta h_b}{h_b}\,(1-\tan\alpha\cot\beta)\right]. \end{aligned} \tag{2.16}$$

At large $\tan\beta$, terms involving $\Delta_b \propto \tan\beta$ [Eq. 2.10] provide the dominant corrections to the neutral Higgs couplings to $b\bar{b}$. The corrections proportional to $\delta h_b/h_b$ [see Eqs. 2.6–2.7 and the discussion that follows] are never $\tan\beta$-enhanced and are therefore numerically unimportant. The τ couplings are obtained from Eq. 2.16 by replacing m_b, Δ_b and δh_b with m_τ, Δ_τ and δh_τ, respectively. Note that Δ_τ and δh_τ arise in analogy with Δ_b and δh_b from SUSY particle loops involving the leptonic sector. In particular, at large $\tan\beta$ [16, 27, 40, 41]:

$$\Delta_\tau \simeq \left[\frac{\alpha_1}{4\pi}M_1\mu I(M^2_{\tilde{\tau}_1},M^2_{\tilde{\tau}_2},M_1^2)-\frac{\alpha_2}{4\pi}M_2\mu\, I(M^2_{\tilde{\nu}_\tau},M_2^2,\mu^2)\right]\tan\beta\,, \tag{2.17}$$

where $\alpha_2 \equiv g^2/4\pi$ and $\alpha_1 \equiv g'^2/4\pi$ are the electroweak gauge couplings. Since corrections to h_τ are proportional to α_1 and α_2, we expect $|\Delta_\tau| \ll |\Delta_b|$. Nevertheless, we shall formally keep the Δ_τ corrections in our analysis, although they will have negligible effect in our numerical results.

To see how the decoupling limit is achieved for the hbb (and $h\tau\tau$) couplings, note that we can write:

$$-\frac{\sin\alpha}{\cos\beta} = \sin(\beta-\alpha) - \tan\beta\cos(\beta-\alpha)\,. \tag{2.18}$$

Working to first order in $\cos(\beta-\alpha)$, and using[12]

$$\tan\alpha\tan\beta = -1 + (\tan\beta+\cot\beta)\cos(\beta-\alpha) + \mathcal{O}\left(\cos^2(\beta-\alpha)\right), \tag{2.19}$$

it follows that

$$g_{hbb} \simeq g_{h_{\rm SM}bb}\left[1-(\tan\beta+\cot\beta)\cos(\beta-\alpha)\left(\sin^2\beta-\frac{\Delta_b-\delta h_b/h_b}{1+\Delta_b}\right)\right]. \tag{2.20}$$

Two points are particularly noteworthy. First, for $m_A \gg m_Z$, decoupling is achieved since $\cos(\beta-\alpha) \sim \mathcal{O}(m_Z^2/m_A^2)$ [Eq. 2.12]. However, because $\Delta_b \propto \tan\beta$, decoupling can be delayed until $m_A^2 \gg m_Z^2\tan\beta$ [44].

[11] We use the notation $\mathrm{BR}(b) \equiv \mathrm{BR}(h\to b\bar{b})$ and $\Gamma(b) \equiv \Gamma(h\to b\bar{b})$, and similarly for other Higgs decay final states.

[12] In the decoupling limit ($m_A \gg m_Z$), Eq. 2.12 implies that that $|(\tan\beta+\cot\beta)\cos(\beta-\alpha)| \ll 1$ for all values of $\tan\beta$.

Second, as noted above, if Eq. 2.14 is satisfied (or equivalently if $c = 0$ [Eq. 2.13]), decoupling is achieved independently of the value of m_A. One also obtains a similar expression for $g_{h\tau\tau}$ by replacing Δ_b and δh_b with Δ_τ and δh_τ in Eq. 2.20. Since $|\Delta_\tau| \ll |\Delta_b|$, it follows that the SM expectation, $g^2_{hbb}/g^2_{h\tau\tau} \propto m_b^2/m_\tau^2$ is violated except in the decoupling limit [15, 16, 43, 51].

Another limiting case of interest is one where $\sin(\beta-\alpha)$ is close to zero. This limit can be reached for values of $m_A \lesssim m_h^{\max}$ and large $\tan\beta$. In this limit, the H couplings to the W and Z bosons approach their Standard Model values and become relevant for our analysis. However, this is not a decoupling limit, and the H couplings to fermion pairs can deviate from the corresponding Standard Model couplings. This can be confirmed by observing that

$$\frac{\cos\alpha}{\cos\beta} = \cos(\beta-\alpha) + \tan\beta\sin(\beta-\alpha)\,. \tag{2.21}$$

But, for large $\tan\beta$, it is possible to have $\tan\beta\sin(\beta-\alpha) \sim \mathcal{O}(1)$ even in the limit of small $\sin(\beta-\alpha)$. Working to first order in $\sin(\beta-\alpha)$ and using

$$\cot\alpha\tan\beta = 1 + (\tan\beta+\cot\beta)\sin(\beta-\alpha) + \mathcal{O}\left(\sin^2(\beta-\alpha)\right)\,, \tag{2.22}$$

it follows that

$$g_{Hbb} \simeq g_{h_{\rm SM}bb}\left[1 - (\tan\beta+\cot\beta)\sin(\beta-\alpha)\left(\cos^2\beta - \frac{1+\delta h_b/h_b}{1+\Delta_b}\right)\right]\,. \tag{2.23}$$

Note that if $|(\tan\beta+\cot\beta)\sin(\beta-\alpha)| \ll 1$, then the Hbb coupling approaches the Standard Model value, even when the Yukawa vertex corrections are included.

We next consider the CP-even Higgs boson couplings to top quark pairs. The analysis is similar to the one given above, and one obtains

$$\begin{aligned} g_{htt} &= \frac{g m_t\cos\alpha}{2m_W\sin\beta}\left[1 - \frac{1}{1+\Delta_t}\frac{\Delta h_t}{h_t}(\cot\beta+\tan\alpha)\right]\,, \\ g_{Htt} &= \frac{g m_t\sin\alpha}{2m_W\sin\beta}\left[1 - \frac{1}{1+\Delta_t}\frac{\Delta h_t}{h_t}(\cot\beta-\cot\alpha)\right]\,. \end{aligned} \tag{2.24}$$

Here, it is more convenient to express our results in terms of Δ_t and $\Delta h_t/h_t$, since $\Delta_t \simeq \delta h_t/h_t$, while the corresponding contribution of $\Delta h_t/h_t$ is $\tan\beta$ suppressed [Eq. 2.8]. The Higgs couplings to charm quark pairs are obtained from Eq. 2.24 by replacing m_t, Δ_t and Δh_t with m_c, Δ_c and Δh_c, respectively. Using $\cot\beta+\tan\alpha \simeq \cos(\beta-\alpha)/\sin^2\beta$ [see Eq. 2.19], it follows that the SUSY vertex corrections to g_{htt} and g_{hcc} are suppressed in the decoupling limit (with no enhancement in the limit of large $\tan\beta$), and so g_{htt} and g_{hcc} approach their Standard Model values. In the opposite limit in which $\sin(\beta-\alpha)$ is close to zero, we use $\cot\beta-\cot\alpha \simeq -\sin(\beta-\alpha)/\sin^2\beta$ [see Eq. 2.22] to conclude that the SUSY vertex corrections to g_{Htt} and g_{Hcc} are suppressed. Thus, in the numerical results presented in this paper, the SUSY Yukawa vertex corrections to both h and H couplings to up-type quark pairs have a negligible effect in the parameter regions of interest and can be neglected.

By considering certain ratios of Higgs-fermion couplings, one can begin to isolate various combinations of SUSY Yukawa vertex corrections. We introduce the notation $\hat{g}_{\phi ff} \equiv g_{\phi ff}/g_{h_{SM}ff}$ [$\phi \equiv h,\, H$] for the Higgs-fermion couplings normalized to their Standard Model values. From Eqs. 2.16 and 2.24, we obtain

$$\frac{\hat{g}_{hbb} - \hat{g}_{h\tau\tau}}{\hat{g}_{htt} - \hat{g}_{hbb}} = \frac{\hat{g}_{Hbb} - \hat{g}_{H\tau\tau}}{\hat{g}_{Htt} - \hat{g}_{hbb}} \simeq \frac{\dfrac{\Delta_b - \Delta_\tau}{1+\Delta_\tau} - \dfrac{\delta h_b}{h_b} + \left(\dfrac{1+\Delta_b}{1+\Delta_\tau}\right)\dfrac{\delta h_\tau}{h_\tau}}{1 - \left(\dfrac{1+\Delta_b}{1+\Delta_t}\right)\dfrac{\Delta h_t}{h_t}\cot\beta + \dfrac{\delta h_b}{h_b}}\,. \tag{2.25}$$

Note that dependence on the CP-even Higgs mixing angle has conveniently canceled out. At large $\tan\beta$, one can to first approximation keep only those terms that are $\tan\beta$-enhanced at one loop. We then obtain:

$$\frac{\hat{g}_{hbb} - \hat{g}_{h\tau\tau}}{\hat{g}_{htt} - \hat{g}_{hbb}} = \frac{\hat{g}_{Hbb} - \hat{g}_{H\tau\tau}}{\hat{g}_{Htt} - \hat{g}_{hbb}} \simeq \frac{\Delta_b - \Delta_\tau}{1+\Delta_\tau} \simeq \Delta_b\,, \tag{2.26}$$

where the last step follows if $|\Delta_\tau| \ll 1$ (we have already noted that $|\Delta_\tau| \ll |\Delta_b|$). Eq. 2.26 and the analogous result in which the Higgs couplings to top quarks are replaced by the corresponding couplings to charm quarks will be used in Sec. 5 when we discuss the extraction of Δ_b from Higgs coupling measurements.

3 Behavior of Higgs decay observables

In this section, we examine in detail the behavior of the MSSM Higgs boson partial widths. In order to present quantitative results, we consider three "benchmark" scenarios for the MSSM parameters that lead to very different behaviors of the SM-like Higgs boson of the MSSM. Our three benchmark scenarios, summarized in Table 1, correspond approximately to those discussed in Ref. [31]. All MSSM parameters are specified at the electroweak scale. The three benchmark scenarios have the following properties:

No-mixing scenario: The top squark mixing angle $\theta_{\tilde{t}}$ is zero. This scenario yields the lowest value of $m_h^{\max}(\tan\beta)$ for given values of $\tan\beta$ and M_S. For simplicity, we define the scenarios in terms of $M_{\rm SUSY} \equiv M_{\tilde{Q}} = M_{\tilde{U}} = M_{\tilde{D}}$, where the latter are third generation squark mass parameters. For $M_{\rm SUSY} \gg m_t$, as is true in the scenarios considered here, $M_{\rm SUSY} \simeq M_S$ [where $M_S^2 \equiv \frac{1}{2}(M_{\tilde{t}_1}^2 + M_{\tilde{t}_2}^2)$]. Here we have chosen a large value for $M_{\rm SUSY} = 1.5$ TeV in order to obtain a sufficiently large value of $m_h^{\max}(\tan\beta)$, comparable to that obtained in the other two scenarios (the case of $M_{\rm SUSY} = 1$ TeV is at the edge of the region excluded by LEP2).

Maximal-mixing scenario: The top squark mixing is chosen to give the maximal value of $m_h^{\max}(\tan\beta)$ for given values of $\tan\beta$ and M_S.

Large μ and A_t scenario: Large radiative corrections occur to both α and Δ_b. In particular, $\mathcal{M}_{12}^2$ can exhibit extreme variations in magnitude depending on the sign of $A_t\mu$ and the magnitude of A_t. The two possible sign combinations for A_t and μ (for a fixed sign of $A_t\mu$) yield small differences in

Mass parameters [TeV]						
Benchmark	μ	$X_t \equiv A_t - \mu \cot\beta$	A_b	$M_{\rm SUSY}$	$M_{\tilde{g}}$	$m_h^{\rm max}$ [GeV]
No-Mixing	-0.2	0	A_t	1.5	1	118
Maximal-Mixing	-0.2	$\sqrt{6}$	A_t	1	1	129
Large μ and A_t	± 1.2	$\mp 1.2(1+\cot\beta)$	0	1	0.5	119

Table 1: MSSM parameters for our benchmark scenarios, and the derived maximal mass for the SM-like Higgs boson.

$\mathcal{M}_{12}^2$ through the dependence of h_t and h_b on Δ_t and Δ_b, respectively. The vertex correction Δ_b is dominated by the bottom squark-gluino contribution, which can enhance or suppress the Yukawa coupling h_b for negative or positive μ, respectively. In the following we choose $A_t\mu < 0$ and consider the two possible sign combinations for A_t and μ.[13]

To be conservative, we have chosen relatively large values for the SUSY breaking parameters, on the order of 1 TeV, so that some supersymmetric particles may not be kinematically accessible at the LC.[14] However, for simultaneously large μ and $M_{\tilde{g}}$, the size of the Δ_b corrections may drive the bottom Yukawa coupling out of the perturbative region. Thus the gluino mass is taken as $M_{\tilde{g}} = 0.5$ TeV for large μ and $M_{\tilde{g}} = 1$ TeV for moderate μ. The other gaugino mass parameters are $M_2 = 2M_1 = 200$ GeV (M_2 is relevant for the one-loop $h \to \gamma\gamma$ amplitude). Finally, the masses of the remaining squarks and sleptons are set to 1 TeV.

We calculate the properties of the MSSM Higgs bosons for each of the benchmark scenarios using the program HDECAY [53], to which we have added the Δ_b and Δ_t Yukawa vertex corrections in the two-loop Higgs boson squared-mass matrix [36] and the Δ_b Yukawa vertex corrections in the Higgs couplings to $b\bar{b}$. By comparing the partial widths, total width and branching ratios of the SM-like Higgs boson of the MSSM and the SM Higgs boson of the same mass, we can evaluate the sensitivity of the various observables for distinguishing the MSSM from the SM. We define the fractional deviations of the MSSM Higgs partial widths from those of the SM Higgs boson of the same mass as follows:

$$\delta\Gamma = \frac{|\Gamma_{\rm MSSM} - \Gamma_{\rm SM}|}{\Gamma_{\rm SM}}\,, \tag{3.1}$$

and analogously for the branching ratios, $\delta{\rm BR} = |{\rm BR}_{\rm MSSM} - {\rm BR}_{\rm SM}|/{\rm BR}_{\rm SM}$. This allows us to demonstrate which Higgs decay quantities are the most sensitive to the non-standard nature of the Higgs boson. Later, we will combine these individual deviations into a χ^2 variable to improve the experimental sensitivity.

[13] If the charged Higgs boson is light, then our choice of the sign of $A_t\mu$ is favored by the experimental constraints on $b \to s\gamma$ [50, 52].

[14] Note that the m_A-independent decoupling in the large μ and A_t scenario depends on μ/M_S and A_t/M_S. Lower values of M_S would allow for correspondingly lower values of μ and A_t.

In the next section, we discuss the expected behavior of the Higgs BRs and partial widths in the MSSM, with particular emphasis on the approach to the decoupling limit [1]. In general, the couplings of the SM-like Higgs boson of the MSSM deviate from those of the SM Higgs boson of the same mass, except in the decoupling limit.

3.1 Theoretical Expectations for Direct Higgs Couplings

Consider first the couplings of the lightest CP-even Higgs boson h to vector bosons ($V = W$ or Z). The corresponding tree-level squared-coupling normalized to the SM value is:

$$\frac{g^2_{hVV}}{g^2_{h_{\rm SM}VV}} = \sin^2(\beta-\alpha)\,. \tag{3.2}$$

To a good approximation, the most important radiative correction to this result can be incorporated by replacing the tree-level value of α by its radiatively-corrected value [obtained in Eq. 2.3]. In the decoupling limit, $\cos(\beta-\alpha)$ is given by Eq. 2.12. It then follows that

$$\frac{g^2_{hVV}}{g^2_{h_{\rm SM}VV}} \simeq 1 - \frac{c^2 m_Z^4 \sin^2 4\beta}{4m_A^4}\,. \tag{3.3}$$

At large $\tan\beta$, the approach to decoupling is even faster, since $\sin 4\beta \simeq -4\cot\beta$ further suppresses the deviation of the partial width $\delta\Gamma(W) = |g^2_{hWW}/g^2_{h_{\rm SM}WW} - 1|$. Contours of $\delta\Gamma(W)$ for the maximal-mixing and large A_t and μ scenarios are shown in the upper left panels of Fig. 1 and Fig. 2. The behavior in the no-mixing scenario is quite similar, and is therefore not shown here explicitly.

We next consider the couplings of h to up-type fermions. At tree-level, we may write (using third-family notation):

$$\frac{g^2_{htt}}{g^2_{h_{\rm SM}tt}} = \left[\sin(\beta-\alpha) + \cot\beta\cos(\beta-\alpha)\right]^2\,, \tag{3.4}$$

where the couplings are expressed in terms of $\sin(\beta-\alpha)$ and $\cos(\beta-\alpha)$ in order to better illustrate the decoupling behavior. Based on the discussion following Eq. 2.24, we may neglect the effects of the SUSY vertex corrections. Then, the dominant radiative corrections can be incorporated simply by employing the radiatively-corrected value of α in the tree-level coupling. Note that the approach to decoupling is significantly slower [by a factor of m_A^2/m_Z^2] than in the case of the hVV coupling [Eq. 3.3]. For example, applying Eq. 3.4 to the Higgs coupling to charmed quarks, one obtains

$$\frac{g^2_{hcc}}{g^2_{h_{\rm SM}cc}} \simeq 1 + \frac{cm_Z^2 \sin 4\beta\cot\beta}{m_A^2}\,. \tag{3.5}$$

At large $\tan\beta$, the approach to decoupling is faster due to the additional suppression factor of $\cot^2\beta$ as in the case of the hVV coupling. The decoupling of $\delta\Gamma(c)$ as m_A increases is exhibited in the upper right panel of Figs. 1 and 2. The behavior in the no-mixing scenario is again similar and is not shown. In

the three benchmarks considered, the W and c couplings to the light Higgs boson decouple quickly for increasing m_A, with a somewhat slower decoupling for the c quark in the low $\tan\beta$ regime.

Finally, we turn to the coupling of h to down-type fermions, and focus on the third-generation $b\bar{b}$ and $\tau^+\tau^-$ decay modes. The approach to the decoupling limit was given for g_{hbb} in Eq. 2.20 [with a similar result for $g_{h\tau\tau}$ easily obtained]. For $m_A \gg m_Z$ (and neglecting $\delta h_b/h_b$ which is not $\tan\beta$-enhanced), it follows that

$$\frac{g^2_{hbb}}{g^2_{h_{\rm SM}bb}} \simeq 1 - \frac{4cm_Z^2\cos 2\beta}{m_A^2}\left[\sin^2\beta - \frac{\Delta_b}{1+\Delta_b}\right]. \tag{3.6}$$

The approach to decoupling is again slower as compared to g_{hVV}. However, in contrast to the previous two cases, there is no suppression at large $\tan\beta$. In fact, since $\Delta_b \propto \tan\beta$, the approach to decoupling is further delayed, unless $c \simeq 0$. Thus, we expect the greatest deviation from the SM in $\delta\Gamma(b)$ and $\delta\Gamma(\tau)$, and this is confirmed in the lower panels of Figs. 1 and 2. As before, the behavior in the no-mixing scenario is quite similar to that of the maximal-mixing scenario and is not shown here. There is a small difference in the behavior of $\delta\Gamma(b)$ with respect to $\delta\Gamma(\tau)$ at large $\tan\beta$ due to the effect of Δ_b, as discussed in Sec. 2. Note that in the large A_t and μ scenario, Fig. 2 exhibits the m_A-independent decoupling phenomenon, corresponding to the case where $c \simeq 0$.[15] If the MSSM parameters are such that the m_A-independent decoupling is realized, then the experimental sensitivity to m_A is greatly compromised. The value of $\tan\beta$ at which this decoupling occurs [Eq. 2.15] depends slightly on the two possible sign choices for μ and A_t (for a fixed value of μA_t) through the dependence of $\delta\mathcal{M}^2_{ij}$ on h_t and h_b (which depend on Δ_t and Δ_b, respectively).

So far, we have discussed the sensitivity of the Higgs couplings to the MSSM parameters. However, experiments at the LC will also measure the Higgs branching ratios. Since $h \to b\bar{b}$ is the dominant decay mode of a Higgs boson lighter than about 135 GeV (unless the $hb\bar{b}$ coupling is anomalously suppressed), $\Gamma(b)$ dominates the total Higgs width. Thus, BR(b) is not as sensitive to deviations of $\Gamma(b)$ from its SM value as the BRs for other decay modes. In particular, since $\Gamma(W)$ quickly approaches its SM value, $\delta{\rm BR}(W) \simeq \delta\Gamma_{\rm tot}$ almost independently of the value of $\tan\beta$. This is illustrated in Fig. 3 for the case of maximal-mixing, and it is generically true in the other benchmark scenarios.

3.2 Loop induced couplings

The decay modes $h \to gg$ and $h \to \gamma\gamma$ proceed only at the loop level. In the MSSM, SUSY particles and additional Higgs bosons also run in the loops. Thus the deviations of $\Gamma(g)$ and $\Gamma(\gamma)$ from their SM values depend not only on deviations in the fermion and W pair couplings to h but also on SUSY loop contributions. $\Gamma(g)$ depends mainly on the t quark loop, which has a SM-like coupling for large m_A except

[15] In principle, this phenomenon could also occur in the case of no-mixing or maximal-mixing. However, in these cases, since $\delta\mathcal{M}^2_{12}$ is quite small, the value of $\tan\beta$ one obtains from Eq. 2.15 would be so large (way beyond what is plotted in Fig. 1 and Fig. 2), that the m_A-independent decoupling takes place in a $\tan\beta$ region that is no longer theoretically meaningful.

at small $\tan\beta$. $\Gamma(\gamma)$ depends mainly on the W boson loop, which has a very rapid decoupling behavior with m_A. Note that, in all the scenarios considered, deviations in the t and c couplings are significant at low $\tan\beta$, and deviations in the b coupling are significant for all $\tan\beta$ values [see Figs. 1 and 2].

For the loop-induced Higgs couplings, there are two separate decoupling limits of relevance. In the first decoupling limit, discussed often in this paper, the non-zero tree-level Higgs couplings approach their SM values for $m_A \gg m_Z$.[16] The second decoupling limit applies to loop-induced Higgs couplings in the limit of large SUSY particle masses. In this limit, the effects of the SUSY-loops decouple, and the loop-induced Higgs couplings are determined by loops of SM particles. If we now take $m_A \gg m_Z$ so that the Higgs couplings to SM particles approach their SM limits, then the resulting loop-induced Higgs coupling should likewise approach its SM limit. However, suppose that $m_A \gg m_Z$ but the masses of some of the SUSY particles that contribute to the loop-induced Higgs couplings are not too large. In this case, the resulting loop-induced Higgs couplings will deviate from the corresponding SM values due to the SUSY loop contributions, which can be a sizable fraction of the SM loop contributions.

In the decay $h \to gg$, the bottom and charm quark contributions destructively interfere with the top quark contribution, reducing the SM amplitude by several percent. Additional deviations arise from squark contributions. The top squark couplings to h are

$$g_{h\tilde{t}_{1,2}\tilde{t}_{1,2}} = g_D - \frac{gm_t^2\cos\alpha}{m_W\sin\beta} \mp \frac{gm_t}{2m_W\sin\beta}\,(\mu\sin\alpha + A_t\cos\alpha)\sin 2\theta_{\tilde{t}}\,, \tag{3.7}$$

where g_D arises from the so-called D-term contribution to the scalar potential.[17] In addition, the minus (plus) sign in Eq. 3.7 corresponds to $h\tilde{t}_1\tilde{t}_1$ ($h\tilde{t}_2\tilde{t}_2$), and $\sin 2\theta_{\tilde{t}} = 2m_tX_t/(M^2_{\tilde{t}_1} - M^2_{\tilde{t}_2})$, where $M_{\tilde{t}_1} < M_{\tilde{t}_2}$. The top-squark contribution to the $h \to gg$ amplitude behaves as $g_{h\tilde{t}_i\tilde{t}_i}/M^2_{\tilde{t}_i}$ for large top squark mass, where the $1/M^2_{\tilde{t}_i}$ suppression is due to the loop integral. This suppression can be partially compensated by a large $h\tilde{t}_i\tilde{t}_i$ coupling. In the decoupling limit [where $\cos(\beta-\alpha) \simeq 0$], it follows that $\mu\sin\alpha + A_t\cos\alpha = \sin\beta X_t$. Thus if X_t is large, the third term in Eq. 3.7 gives a contribution to the $h \to gg$ amplitude proportional to $m_tX_t\sin 2\theta_{\tilde{t}}/M^2_{\tilde{t}_i}$ [i = 1,2]. Note that if $|X_t| \sim M_{\tilde{t}_i}$ and the diagonal elements of the top squark squared-mass matrix are of the same order, then $|\sin 2\theta_{\tilde{t}}| \simeq 1$ and this contribution to the amplitude decouples like $m_t/M_{\tilde{t}_i}$, *i.e.*, suppressed by one power of $M_{\tilde{t}_i}$. This should be contrasted with the case of small top-squark mixing angle (*i.e.*, $|\sin 2\theta_{\tilde{t}}| \ll 1$), which arises when m_tX_t is small compared to the difference of the diagonal entries of the squark squared-mass matrix. In this case, the dominant contribution to the

[16] In principle, deviations can arise from radiative corrections due to loops of SUSY particles, but these corrections will be a small fraction of the corresponding SM tree-level Higgs coupling.

[17] Explicitly, $g_D \equiv gm_Z(1 \mp (\frac{8}{3}\sin^2\theta_W - 1)\cos 2\theta_{\tilde{t}})\sin(\alpha+\beta)/4\cos\theta_W$. This term is independent of m_t and gives rise to a small coupling of h to all squark species, independent of the corresponding quark Yukawa coupling, so that the squarks of the first two generations also contribute to $h \to gg$. Thus, in our numerical calculations we must specify the masses of the squarks of the first two generations; we set $M_{\tilde{Q}} = M_{\tilde{U}} = M_{\tilde{D}} = 1$ TeV in all cases, as mentioned before. With this choice, the contributions of the first two generations of squarks are negligible.

$h\tilde{t}_i\tilde{t}_i$ couplings comes from the second term in Eq. 3.7, and the top squark loop contribution to the $h \to gg$ amplitude decouples like $m_t^2/M_{\tilde{t}_i}^2$. This behavior of the top squark contribution with X_t explains the behavior of $\Gamma(g)$ in the no-mixing and maximal-mixing scenarios (the top panels of Fig. 4). At low m_A, the $hb\bar{b}$ coupling is enhanced over its SM value so that $\Gamma(g)$ is suppressed due to the destructive interference between the bottom quark and top quark loops. In the no-mixing scenario, the top squark contribution enters with the same sign as the dominant top quark loop; as m_A increases, the b quark contribution approaches its SM value and the top squark contribution then leads to a small enhancement of $\Gamma(g)$ at large m_A. Thus in the no-mixing scenario (the top left panel of Fig. 4) we see that $\Gamma_{\rm MSSM}(g) - \Gamma_{\rm SM}(g)$ passes through zero for $m_A \sim 0.6-1$ TeV and reaches an asymptotic value of 1–2% in the large m_A limit. In the maximal-mixing scenario, the top squark loop contribution is enhanced by the large value of X_t and enters with the opposite sign as the dominant top quark loop; thus it leads to a further suppression of $\Gamma(g)$ in addition to the suppression due to the enhanced $hb\bar{b}$ coupling at low m_A. As m_A increases, then, the b quark contribution approaches its SM value and $\delta\Gamma(g)$ reaches an asymptotic value of about 6% in the large m_A limit, without $\Gamma_{\rm MSSM}(g) - \Gamma_{\rm SM}(g)$ passing through zero at any value of m_A.

In the large μ and A_t scenarios, the behavior of $\Gamma(g)$ is more complicated. At low $\tan\beta$, the behavior of $\delta\Gamma(g)$ is dominated by the decoupling behavior of the $ht\bar{t}$ coupling (see Fig. 2). At large $\tan\beta$, m_A-independent decoupling effects and Δ_b play an important role. For $\mu < 0$ (shown in the bottom right panel of Fig. 4), $\delta\Gamma(g)$ is quite significant at large $\tan\beta$, and the deviations from the SM in this region are independent of m_A for $m_A \gtrsim 0.5$ TeV. For this sign of μ, Δ_b is large and negative (the two terms in Eq. 2.10 enter with the same sign), resulting in a significant enhancement of h_b in the large $\tan\beta$ region. Because of this enhancement of h_b, the bottom squark loop contributions are significant in this scenario at large $\tan\beta$; they modify the $h \to gg$ amplitude by a few percent, leading to several percent deviations in $\Gamma(g)$. At lower values of m_A, the b quark loop also contributes due to the deviation in the $hb\bar{b}$ coupling (see Fig. 2). For $\mu > 0$ (the bottom left panel of Fig. 4), $\delta\Gamma(g)$ exhibits m_A-independent decoupling for $\tan\beta \simeq 40$. For this sign of μ, the two terms contributing to Δ_b in Eq. 2.10 enter with opposite signs, leading to a partial cancellation, and the overall sign of Δ_b is positive. Thus Δ_b leads to a small suppression of h_b, and the bottom squark loop contribution is not significant.

Contours of $\delta\Gamma(\gamma)$ are shown in Fig. 5. In the SM, $\Gamma(\gamma)$ is dominated by the W boson contribution; at low $m_A \lesssim 0.2$ TeV, the deviation of $\Gamma(\gamma)$ from its SM value is dominated by the deviation of the hWW coupling (see Figs. 1 and 2). Because this one-loop decay gets contributions from all charged particles that couple to h, it depends not only on the parameters of the squark and slepton sectors but also on the charginos. It was shown in Ref. [54] that near the decoupling regime, only top and bottom squark and chargino contributions can generate a sizable deviation from the SM partial width. In the no-mixing and maximal-mixing scenarios, we choose $M_2 = -\mu = 200$ GeV. This choice leads to large Higgsino-gaugino mixing, so that the couplings of h to chargino pairs are large. Thus at low $\tan\beta$ and $m_A \gtrsim 0.2$ TeV, the

chargino contribution to $\delta\Gamma(\gamma)$ is responsible for the bulk of the deviation from the SM. As $\tan\beta$ increases, the Higgsino-gaugino mixing decreases and the chargino contribution becomes smaller (see the top two panels of Fig. 5). As in the case of $h \to gg$, there are also top squark contributions to $h \to \gamma\gamma$; these are very small in the no-mixing scenario but somewhat larger in the maximal-mixing scenario due to the large X_t enhancement of the $h\tilde{t}_i\tilde{t}_i$ couplings, as discussed before. In the maximal-mixing scenario, the top squark and chargino contributions to the amplitude enter with opposite signs. Then as $\tan\beta$ increases, the chargino contribution shrinks until it is the same size as the top squark contribution; this occurs for $\tan\beta \simeq 15 - 20$, where $\delta\Gamma(\gamma)$ goes to zero in this scenario. At larger values of $\tan\beta$, the top squark contribution is responsible for the bulk of the deviation from the SM. In the large μ and A_t scenarios (the bottom two panels of Fig. 5), we have $M_2 \ll |\mu|$, so that the Higgsino-gaugino mixing is very small and the couplings of h to chargino pairs are suppressed. Thus in these scenarios the chargino contribution is very small, and appears only at low $\tan\beta$. For $\mu < 0$, the deviation at very large $\tan\beta$ and low m_A is due to the deviation in the $hb\bar{b}$ coupling in the b quark loop, as in the case of $h \to gg$.

4 Higgs boson measurements at future colliders

Figs. 1–5 demonstrate our theoretical expectations for the behavior of partial widths and branching ratios in the MSSM with respect to the SM. In this section, we fold those results with the expected experimental resolution from the next generation of experiments at linear colliders and compare it to what will be known from hadron collider experiments.

4.1 Anticipated experimental uncertainties in Higgs branching ratios and couplings

We expect quite sensitive measurements at the LC of both the Higgs production cross sections and the BRs for the most important Higgs boson decay modes. Combining these measurements, it is possible to extract the total Higgs boson width and the partial widths for the various decay modes. The measurement of the total cross section for $e^+e^- \to Zh$ yields a measurement of g^2_{hZZ}. Branching ratios are determined by selecting Higgs events in Zh production, where $Z \to \ell^+\ell^-$, using the recoil mass technique and counting the different types of events in the invariant mass region of the Higgs boson signal. These branching ratio determinations are model independent, even if invisible Higgs decays are present. Finally, by including other Z decay modes in hZ production as well as Higgs production via vector boson fusion, one can further improve the statistical precision of the Higgs branching ratios and Higgs couplings.

The expected experimental uncertainties in the measurement of BRs at the LC for a 120 GeV SM-like Higgs boson are summarized in Table 2. The first row shows the results assuming 500 fb^{-1} of integrated luminosity at $\sqrt{s} = 350$ GeV [7]. At $\sqrt{s} = 500$ GeV, the $e^+e^- \to Zh$ cross section for $m_h = 120$ GeV is about a factor of two smaller than at 350 GeV [55]; thus roughly twice as much integrated luminosity

Decay mode:	$b\bar{b}$	WW^*	$\tau^+\tau^-$	$c\bar{c}$	gg	$\gamma\gamma$
Ref. [7]	2.4%	5.1%	5.0%	8.5%	5.5%	19%
Ref. [12]	2.9%	9.3%	7.9%	39%	18%	
Ref. [13] (scaled)						14%
theory uncertainty	1.4%	2.3%	2.3%	23%	5.7%	2.3%

Table 2: Expected fractional uncertainty of BR measurements at an e^+e^- LC for a 120 GeV SM-like Higgs boson. Results are shown from Ref. [7] (500 fb^{-1} at $\sqrt{s} = 350$ GeV) (first row); Ref. [12] (500 fb^{-1} at $\sqrt{s} = 500$ GeV) (second row); and Ref. [13] (1 ab^{-1} at $\sqrt{s} = 500$ GeV, scaled to 500 fb^{-1}) (third row). The theoretical uncertainty of the predicted Standard Model branching ratios is given in the fourth row (see Sec. 4.2).

(*i.e.*, about 1 ab^{-1}) would be needed at 500 GeV to obtain the same statistical precision on Higgs BRs. To estimate the precision on Higgs BRs that can be obtained with 500 fb^{-1} at $\sqrt{s} = 500$ GeV, the results for $\sqrt{s} = 350$ GeV shown on the first line of Table 2 should be reduced by a factor of 1.5 (corresponding to the square root of the ratio of the corresponding Zh cross sections for $m_h = 120$ GeV).[18] The second row of Table 2 shows the results of a similar study [12] for the branching ratios of a 120 GeV SM-like Higgs boson with 500 fb^{-1} at $\sqrt{s} = 500$ GeV.[19] Finally, we consider the results of a dedicated study of the BR(γ) measurement [13] for $\sqrt{s} = 350$ and 500 GeV, both without and with beam polarization (80% left-handed electron polarization and 40 or 60% right-handed positron polarization) chosen to enhance the Higgsstrahlung and WW fusion cross sections. At $\sqrt{s} = 500$ GeV and the highest polarizations, a measurement of BR(γ) with an experimental uncertainty of 9.6% is possible with 1 ab^{-1}. Scaling this to 500 fb^{-1} to compare with the other studies yields a precision of about 14%, as shown in the third row of Table 2. Without beam polarization, this deteriorates to 16% (23%) with 1 ab^{-1} (500 fb^{-1}).

The $\delta\Gamma(\gamma)$ deviations shown in Fig. 5 are typically too small to be observed at an e^+e^- linear collider. However, the operation of the LC as a photon-photon collider offers the possibility of a direct measurement of $\Gamma(\gamma)$ from the s-channel Higgs production cross section $\sigma(\gamma\gamma \to h)$. Estimates for the precision obtainable on $\sigma(\gamma\gamma \to h) \times \mathrm{BR}(h \to b\bar{b})$ range from 2–10% for a light Higgs boson with mass between 120 and 160 GeV [20] from a $\gamma\gamma$ collider running at $\sqrt{s_{ee}} \simeq m_h/0.8$ (giving peak $\gamma\gamma$ luminosity at the Higgs mass) and an integrated luminosity corresponding to 400 fb^{-1} of e^-e^- luminosity [57]. Combining a 2% measurement of $\sigma(\gamma\gamma \to h) \times \mathrm{BR}(h \to b\bar{b})$ at a $\gamma\gamma$ collider for a 120 GeV Higgs boson with a 3% measurement of

[18] This scaling is only approximate since it does not take into account the Higgs production by vector boson fusion employed in the analysis of Ref. [7].

[19] Note the very different predictions in Table 2 for the precisions of BR(c) and BR(g), which depend on very good charm and light quark separation. The authors of Refs. [7] and [12] are working together to resolve these discrepancies [56].

[20] The variation in precision is due to the decline of BR($h \to b\bar{b}$) as m_h increases.

	g^2_{hbb}	g^2_{hWW}	g^2_{hZZ}	g^2_{hcc}	$g^2_{h\tau\tau}$	g^2_{hgg}	g^2_{htt}
experimental uncertainty	4.4%	2.4%	2.4%	7.4%	6.6%	7.4%	10%
theory uncertainty	3.5%	–	–	24%	–	3.9%	2.5%

Table 3: Expected uncertainty of measurements of squared couplings (equivalently partial widths) for a 120 GeV SM-like Higgs boson from HFitter [7,59], assuming 500 fb^{-1} at $\sqrt{s} = 500$ GeV, except for the measurement of g^2_{htt} which assumes 1000 fb^{-1} at $\sqrt{s} = 800$ GeV. The second line shows the theoretical uncertainty (see Sec. 4.2).

BR($h \to b\bar{b}$) at the e^+e^- LC, we find that $\Gamma(\gamma)$ could be extracted with an uncertainty of about 3.6%. As Fig. 5 shows, such a measurement would not exhibit a significant deviation from the SM prediction in our benchmark scenarios unless $m_A \lesssim 200$ GeV or $\tan\beta$ is very small; however, a more detailed analysis of the MSSM parameter space should be performed in light of this expected precision.

From the measurement of g^2_{hWW} based on the production cross section, the partial width $\Gamma(W)$ can be calculated and combined with the measurement of BR(W) to determine the total Higgs width $\Gamma_{\rm tot}$. The expected resolution on g^2_{hZZ} of about 3% yields a measurement of the total width to roughly 6% accuracy [7,55]. This method for extracting the total Higgs width is more accurate than using the photon collider mode.[21] However, the photon collider mode is still quite useful for the high precision measurement that it provides of the partial width $\Gamma(\gamma)$. In other models, such as the (non-SUSY) two Higgs doublet model, this measurement can be essential for distinguishing the extended model from the SM in some regions of parameter space [58].

Combining the measurements of Higgs boson BRs and production cross sections that can be obtained at the LC, the Higgs couplings to SM particles can be extracted [55]. The results of a χ^2 minimization using HFitter [7,59] are summarized in Table 3. The first six couplings listed in Table 3 are extracted from h BRs into $b\bar{b}$, WW^*, $c\bar{c}$, $\tau\tau$ and gg and the production cross sections in the Higgsstrahlung and WW fusion modes, assuming 500 fb^{-1} at $\sqrt{s} = 500$ GeV [the first five of these are given in Ref. [55]]. The $ht\bar{t}$ coupling can be measured indirectly from the LC measurements of $h \to gg$ and $h \to \gamma\gamma$ if one assumes that SUSY loop contributions are negligible; however, this is a model-dependent assumption that we wish to avoid. A direct measurement of g^2_{htt} can be obtained from the $e^+e^- \to t\bar{t}h$ cross section [55,60]. Such a measurement requires running at higher $\sqrt{s} = 800-1000$ GeV in order to avoid kinematic suppression of

[21] As noted earlier, $\Gamma(\gamma)$ can be measured to about 3–4% accuracy in $\gamma\gamma$ collisions. The total Higgs width is then extracted by combining this measurement with BR(γ). Using the range of uncertainties in BR(γ) given in Table 2, we see that the uncertainty in the total Higgs width extracted by this method is dominated by the large uncertainty in BR(γ). This can be improved somewhat by combining the LC measurements and the LHC data on $\Gamma(\tau)/\Gamma(\gamma)$ (see Table 4), as discussed at the end of Sec. 4.5. Even in this case, the uncertainty in BR(γ) still dominates the total Higgs width as extracted from the $\gamma\gamma$ collider measurements.

the cross section; the result in Table 3 assumes 1000 fb^{-1} at $\sqrt{s} = 800$ GeV. [22] The studies summarized in Tables 2 and 3 were conducted for the SM Higgs boson of mass 120 GeV, and thus are directly applicable to the study of a SM-like Higgs boson of the MSSM with a mass near 120 GeV, especially near the decoupling limit. In our benchmark scenarios, the value of m_h varies between 118 and 129 GeV. We shall assume that the mass dependence of the results quoted in Tables 2 and 3 is minimal in this mass range, but this assumption should be tested with detailed simulations.

4.2 Theoretical uncertainties in Higgs branching ratios and couplings

In order to gauge the significance of an observed deviation of Higgs boson properties at the LC from the Standard Model expectation, one must take into account both the experimental uncertainties (statistical and systematic) described in Sec. 4.1 and the corresponding theoretical uncertainties for the Standard Model Higgs boson. Sources of theoretical uncertainty include higher order loop corrections to Higgs decay rates not yet computed and parametric uncertainties due to the choice of input parameters. The largest sources of uncertainty arise from the choice of α_s, m_c and m_b.[23] To determine the current theoretical uncertainty in Higgs branching ratios and couplings, we choose $\alpha_s = 0.1185 \pm 0.0020$ [61], $m_c(m_c) = 1.23 \pm 0.09$ GeV [62] and $m_b(m_b) = 4.17 \pm 0.05$ GeV [63] (see Ref. [64] for an alternative evaluation of $\overline{\rm MS}$ quark masses). By varying these input parameters in the program HDECAY [53], we obtain the theoretical fractional uncertainties for the Higgs branching ratios quoted in Table 2. For the Higgs squared-couplings listed in Table 3, the only significant theoretical uncertainties reside in g^2_{hbb} and g^2_{hcc}, due to the uncertainties in the b and c quark masses and in α_s (which governs the running of the quark masses from the quark mass to the Higgs mass). The resulting theoretical uncertainties for g^2_{hbb} and g^2_{hcc} (for a SM Higgs boson of mass 120 GeV) are 3.5% and 24%, respectively. In addition, we find a theoretical uncertainty in g^2_{hgg} of 3.9% due to the uncertainty in α_s.

For a SM Higgs boson with $m_h = 120$ GeV, about 2/3 of the width is due to $h \to b\bar{b}$. The theoretical fractional uncertainties for the Higgs branching ratios to WW^*, $\tau^+\tau^-$ and $\gamma\gamma$ listed in Table 2 are due primarily to the fractional uncertainty of the total width, which for a SM Higgs boson with $m_h = 120$ GeV is mainly governed by the corresponding uncertainty in the $h \to b\bar{b}$ width.[24] The theoretical uncertainty in the $h \to c\bar{c}$ decay rate is particularly large due to the relatively large uncertainty in the charmed quark mass. It is hoped that further theoretical work and numerical improvements in lattice calculations [65] will

[22] The experimental uncertainty in g^2_{htt} can be reduced by combining the $e^+e^- \to t\bar{t}h$ cross section measurement with the measurements of $h \to gg$ and $h \to \gamma\gamma$ if one assumes that SUSY loop contributions to the latter are negligible; the resulting uncertainty in g^2_{htt} is 6.0% [55].

[23] The observed uncertainty in m_t has only a small effect on the predictions for the $h \to gg$ and $h \to \gamma\gamma$ decay rates. This is not surprising given that the top quark mass is the most accurately known of all the quark masses!

[24] For larger values of the Higgs mass, the $h \to b\bar{b}$ branching ratio is smaller and the uncertainty in the total width, which is now dominated by $h \to WW^{(*)}$, is correspondingly reduced.

reduce this theoretical uncertainty by the time that LC data is available.

Finally, a scan of the $t\bar{t}$ threshold at the LC will yield a value of m_t with an uncertainty of about 100 MeV [66]. Thus, the theoretical error expected for the Standard Model Higgs coupling to $t\bar{t}$ due to the top-quark mass uncertainty will be negligible. The remaining uncertainty in g^2_{htt} is due to uncalculated higher order QCD corrections to the $e^+e^- \to t\bar{t}h$ cross section. We estimate this uncertainty to be about 2.5% based on the renormalization scale dependence in the next-to-leading order (NLO) QCD result for $m_h = 120$ GeV and $\sqrt{s} = 1$ TeV [67].

4.3 Branching ratio analysis

A number of the Higgs BRs can be measured to higher accuracy than the total Higgs width. Thus BR measurements alone are valuable for distinguishing the SM Higgs boson from a MSSM Higgs boson. To illustrate the potential of the LC, contours of δBR (Eq. 3.1) are shown in Fig. 6 over the m_A—$\tan\beta$ plane for the benchmark scenarios. Contours of $\delta\mathrm{BR}(b) = 3$ and 6% and $\delta\mathrm{BR}(W)$, $\delta\mathrm{BR}(g) = 8$ and 16% were chosen, corresponding roughly to one and two times the expected experimental uncertainties quoted in Table 2, or approximately one and two sigma deviations from the SM.[25] As shown in Table 2, the theoretical uncertainties in these three BRs for the SM Higgs boson are smaller than the expected experimental uncertainties.

In the four panels of Fig. 6, the solid, long-dashed, and short-dashed lines are contours of $\delta\mathrm{BR}(b)$, $\delta\mathrm{BR}(W)$ and $\delta\mathrm{BR}(g)$, respectively. Although $\delta\Gamma(b)$ is quite large over much of the parameter space, $\delta\mathrm{BR}(b)$ is smaller because the increase in $\Gamma(b)$ also significantly increases Γ_{tot}. Because $\delta\Gamma(W)$ quickly approaches zero for increasing m_A, $\delta\mathrm{BR}(W)$ indicates variation in the total Higgs width, and is more sensitive than $\delta\mathrm{BR}(b)$, except for the case of maximal mixing. In regions of parameter space where $\delta\Gamma(g)$ approaches zero (see Fig. 4), $\delta\mathrm{BR}(g)$, like $\delta\mathrm{BR}(W)$, is sensitive to variations in the total width.

For the maximal-mixing scenario, the mass of the SM-like Higgs boson near the decoupling limit is roughly 10 GeV heavier than in the other benchmarks (see Table 1), so that the relative contribution of $\Gamma(b)$ to Γ_{tot} is decreased. Therefore, deviations in g_{hbb} are not as diluted in the BR measurement as in the other scenarios, and the measurement of $\delta\mathrm{BR}(b)$ yields superior sensitivity at large $\tan\beta$, around $m_A \lesssim 600$–700 GeV at 2σ. One should interpret this result with caution, however, since the accuracies for BR measurements are based on the simulation of a 120 GeV SM Higgs boson. In the maximal-mixing scenario, $\mathrm{BR}(g)$ deviates by more than 8% from its SM value for $m_A \lesssim 1.4$ TeV. At 2σ the reach in $\delta\mathrm{BR}(g)$ is roughly $m_A \lesssim 600$ GeV. In the no-mixing scenario, $\delta\mathrm{BR}(g)$ and $\delta\mathrm{BR}(W)$ give comparable reach in m_A; at 2σ the reach is $m_A \lesssim 425$ GeV. For comparison, in the no-mixing scenario deviations in $\mathrm{BR}(b)$ yield sensitivity at 2σ for $m_A \lesssim 300$ GeV for $\tan\beta \gtrsim 5$.

[25] We choose typical values rather than using the precisions quoted in the experimental studies [7, 12] because we expect the exact results of these studies to change as the LC detector design evolves and experimental techniques improve.

The large μ and A_t scenario demonstrates the complementarity of the LC and the hadron colliders. For $\tan\beta \lesssim 20$, where the heavy MSSM Higgs bosons can be missed at the LHC, BR(g) gives the greatest reach in m_A, allowing one to distinguish the MSSM from the SM Higgs boson at 2σ for $m_A \lesssim 350$–450 GeV, depending on the value of $\tan\beta$. At larger values of $\tan\beta$, the large μ and A_t scenarios have regions of m_A-independent decoupling where the SM-like MSSM Higgs boson cannot be distinguished from the SM Higgs boson even for very low values of m_A. In fact, in these scenarios it is possible for h to be indistinguishable from the SM Higgs boson at the LC, while at the same time $m_A < 250$ GeV so that the heavy Higgs bosons will be directly observed at a 500 GeV LC through $e^+e^- \to HA$, H^+H^-. Moreover, in our scenarios with $A_t\mu < 0$, for $\mu > 0$ [$\mu < 0$] the m_A-independent decoupling occurs for $\tan\beta \simeq 40$ [$\tan\beta \simeq 33$].[26] For such large values of $\tan\beta$, the heavy MSSM Higgs bosons would be discovered at the LHC even for m_A above 500 GeV [3]. Note also that for large μ and A_t and large $\tan\beta$, the correction Δ_b is quite large, and modifies the b quark Yukawa coupling from its SM value. The effect of Δ_b on the couplings of the heavy MSSM Higgs bosons does *not* decouple for $m_A \gg m_Z$ (*i.e.*, for $\tan\alpha\tan\beta = -1$). Thus Δ_b could have a significant effect on the discovery of the heavy Higgs bosons at the Tevatron and LHC in this region of parameter space by modifying their production cross sections and decay branching ratios. In particular, the value of $\tan\beta$ extracted from the A and H production rates at the LHC [3] could not be unambiguously determined without knowledge of the value of Δ_b. LC data would then be of great value for disentangling the Δ_b dependence (see Sec. 5) so that the value of $\tan\beta$ extracted from heavy Higgs boson measurements can be compared to the value obtained from other sectors of the theory.

Clearly, from Fig. 6, the regions of the m_A—$\tan\beta$ plane in which the MSSM and SM Higgs bosons can be distinguished from one another depend strongly on the supersymmetric parameters, and the sensitivity comes from different measurements for different sets of MSSM parameters. In isolation, measurements of one or two sigma deviations in individual BRs would not be a significant probe of the MSSM. In combination, however, the measurements are much more powerful, as indicated by the χ^2 analysis presented in the next section.

4.4 χ^2 analysis of couplings

In order to make a quantitative assessment of the ability of the LC to discriminate between the SM-like Higgs boson of the MSSM and the SM Higgs boson, we combine several observations and compute the compatibility with the SM using a χ^2 test. In particular, $\chi^2 = \sum_i (X_i^{\rm MSSM} - X_i^{\rm SM})^2/\sigma_i^2$, where i is a decay product and X is a BR, Γ, a Higgs squared-coupling or a ratio of these quantities. The σ_i values include the experimental resolution and any theoretical uncertainty on the quantity X_i. Motivated by the HFitter results [55], we choose the X_i to be the squared couplings of Higgs bosons to various final

[26] As explained in Sec. 3.1, the value of $\tan\beta$ at which this m_A-independent decoupling occurs has a small dependence on the signs of μ and A_t.

states. The significance of a particular value for χ^2 depends on the number of observables that have been combined. Our results indicate that the addition of several variables does not necessarily improve the significance. For example, the $h\gamma\gamma$ coupling is not measured very well, and the relative theoretical error in the predicted $hc\bar{c}$ coupling is too large. Moreover, the hWW and $hc\bar{c}$ couplings quickly approach their SM values for increasing m_A. Thus measurements of these three couplings do not add to the significance of our results. Therefore, we compute the χ^2 combining $b\bar{b}$, $\tau^+\tau^-$ and gg squared-coupling measurements, adding in quadrature the experimental and theoretical uncertainties in each squared-coupling [see Table 3].

The χ^2 results are shown in Fig. 7 for the benchmark scenarios with contours corresponding to $68, 90, 95, 98$ and 99% confidence levels. For $\tan\beta \gtrsim 5$, the no-mixing and maximal-mixing scenarios can be distinguished from the SM at 95% [99%] confidence level for $m_A \lesssim 600$ [500] GeV and 650 [600] GeV, respectively. The large A_t and μ scenarios have regions at some large $\tan\beta$ values that are indistinguishable from the SM for any value of m_A. For $\tan\beta \lesssim 20$, however, the large μ and A_t scenarios can be distinguished from the SM at 95% [99%] confidence level for $m_A \lesssim 450$ [425] GeV. Note also that for $\mu < 0$, the large Δ_b effects lead to significant deviations from the SM even for $m_A \lesssim 2$ TeV at the largest values of $\tan\beta$.

4.5 Complementarity to hadron collider measurements

Measurements of Higgs boson properties will be available from the Tevatron and the LHC. This data will most likely be available before the LC is operational. Based on our current understanding of the MSSM Higgs boson properties and experimental capabilities, these hadron colliders will observe a light, SM-like Higgs boson and, perhaps, other non-SM-like Higgs bosons if their couplings to heavy flavor are enhanced over the SM (*e.g.*, H and A will be observed in $b\bar{b}H/A$ if $\tan\beta$ is sufficiently large [2, 3]).

If a light, SM-like Higgs boson is discovered, various combinations of production cross sections times branching ratios will be measured at the LHC to about 10–20% [68] assuming an integrated luminosity of 100 fb^{-1} at each of the two detectors. The uncertainties on most of these measurements are dominated by statistical error. From these measurements, various ratios of the partial widths of a 120 GeV SM-like Higgs boson to ZZ^*, WW^*, $\gamma\gamma$, $\tau^+\tau^-$, and gg can be extracted with uncertainties between 15 and 30%. Expected uncertainties from Ref. [68] are summarized in Table 4,[27] along with the corresponding uncertainties from LC measurements with 500 fb^{-1} at $\sqrt{s} = 350$ GeV [7] and from HFitter [7, 59] at the LC with 500 fb^{-1} at $\sqrt{s} = 500$ GeV.

Assuming that the hWW and hZZ couplings are related by the usual SU(2) relation, that $\Gamma(b)$ is related to $\Gamma(\tau)$ by the SM relation, and that only the decay modes $b\bar{b}$, ZZ^*, WW^*, $\gamma\gamma$, $\tau^+\tau^-$, and gg are needed to estimate the total Higgs width, then $\Gamma(W)$ and $\Gamma_{\rm tot}$ can also be extracted from LHC measurements

[27] The decay modes to $\gamma\gamma$, ZZ^* and WW^* were considered for inclusive Higgs production (dominated by gluon fusion) and the decay modes $\gamma\gamma$, $\tau^+\tau^-$ and WW^* were considered for Higgs production through vector boson fusion.

	$\Gamma(Z)/\Gamma(W)$	$\Gamma(\gamma)/\Gamma(W)$	$\Gamma(\tau)/\Gamma(W)$	$\Gamma(\tau)/\Gamma(\gamma)$	$\Gamma(g)/\Gamma(W)$	$\Gamma(b)/\Gamma(W)$
LHC [68]	29%	16%	15%	15%	15%	–
LC [7]	–	20%	7.1%	20%	7.5%	5.6%
HFitter [55]	3.4%	–	6.6%	–	–	2.4%

Table 4: Expected uncertainties for the ratios of partial widths of a 120 GeV SM-like Higgs boson from the LHC [68] (100 fb^{-1} at each of the two detectors), the e^+e^- LC [7] (ratios of BRs; 500 fb^{-1} at $\sqrt{s} = 350$ GeV), and the e^+e^- LC using HFitter [7, 55, 59] (500 fb^{-1} at $\sqrt{s} = 500$ GeV).

with uncertainties of 10 and 20%, respectively [68]. (The second assumption is violated by the Δ_b Yukawa vertex corrections; this affects the determination of both $\Gamma(W)$ and $\Gamma_{\rm tot}$.) The branching ratio for the decay to $b\bar{b}$ is more difficult to measure at the LHC due to QCD backgrounds. $\Gamma(b)$ can be extracted to about 50% from vector boson fusion $Whjj$ events [69].

From Table 4, it is clear that LC measurements would give a significant improvement over the hadron collider measurements. The LC also offers the advantage of model-independent measurements of the Higgs boson branching ratios, even if invisible Higgs boson decays are present, and a model-independent determination of the Higgs total width. Generally speaking, except for the rare $\gamma\gamma$ decay, the LC has measurement uncertainties that are smaller by at least a factor of 2 compared to the LHC. The precision of $b\bar{b}$ measurements are improved by an order of magnitude at the LC.

Some information may also be available from the hadron colliders regarding m_A or $m_{H^\pm}$ and $\tan\beta$ [5]. For example, if the SUSY spectrum is such that Δ_b and Δ_τ are negligible, then $\tan\beta$ can be measured at the LHC from $b\bar{b}H/A$, $H/A \to \tau^+\tau^-$ event rates with a 5–25% statistical uncertainty and about a 10% luminosity uncertainty [3, 70]. However, as indicated earlier, the extraction of $\tan\beta$ from LHC Higgs boson measurements will require knowledge of Δ_b and Δ_τ. Moreover, several interpretations of high-mass excesses of τ's may exist, especially within the MSSM at large $\tan\beta$. As we have discussed already, in most regions of parameter space the LC can provide an indirect measurement of m_A for values of m_A significantly beyond the $e^+e^- \to AH$ kinematic limit.

From Tables 2 and 4, we see that the combination of LHC and LC measurements will significantly improve our knowledge of BR(γ) in the absence of a $\gamma\gamma$ collider. In particular, the ratio of Higgs partial widths $\Gamma(\tau)/\Gamma(\gamma)$ can be determined to 15% accuracy using ratios of production cross sections times branching ratios in Higgs production through vector boson fusion. Combining this with the LC measurement of BR(τ) to 5–8%, we find that BR(γ) can be extracted with a precision of 16–17%. If the BR(γ) measurement at the LC of 14–19% is combined with this BR(γ) extraction from LHC data, a "world average" precision of 11–13% can be obtained.

5 Extracting SUSY parameters: Δ_b

In this section we examine the possibility of extracting MSSM parameters from measurements of the properties of the SM-like Higgs boson. We concentrate on the SUSY vertex corrections to the $hb\bar{b}$ coupling, Δ_b (see Sec. 2). As noted in Sec. 4.3, when Δ_b is large it can have a significant effect on the phenomenology of the heavy MSSM Higgs bosons. In particular, at large $\tan\beta$, knowledge of Δ_b will be needed to extract the value of $\tan\beta$ from measurements of the A and H production rates at the LHC [3]. Because Δ_b depends on a combination of MSSM parameters (Eq. 2.10), a measurement of this quantity provides a constraint on MSSM parameter space. However, additional information is needed to fully disentangle these parameters; *e.g.*, the gluino and bottom squark masses can be obtained from measurements at hadron colliders. To extract Δ_b directly from the data in the large $\tan\beta$ regime, we shall consider the following ratio of Higgs couplings [see Eq. 2.26]

$$\frac{\hat{g}_{hbb} - \hat{g}_{h\tau\tau}}{\hat{g}_{htt} - \hat{g}_{hbb}} \simeq \frac{\hat{g}_{hbb} - \hat{g}_{h\tau\tau}}{\hat{g}_{hcc} - \hat{g}_{hbb}} \simeq \Delta_b \,, \tag{5.1}$$

where we have employed the notation introduced at the end of Sec. 2 for Higgs-fermion couplings normalized to their Standard Model values.

At the LC the $hb\bar{b}$ and $h\tau\tau$ couplings can be extracted from measurements of BR(b), BR(τ) and the total width of h, as discussed in Sec. 4.1. In the up-type quark sector, the measurements of h couplings to charm- and top-quark pairs are possible at the LC. In h decays, we have access to the $hc\bar{c}$ coupling through BR(c). This measurement, like those of the $hb\bar{b}$ and $h\tau\tau$ couplings, can be made in the initial stage of the LC running at $\sqrt{s} = 350$ or 500 GeV. However, as discussed in Sec. 4.2, the theoretical uncertainty in $g_{h_{SM}cc}$ is very large due to the large uncertainty in the charm quark mass. If the uncertainty in the charm quark mass is not significantly reduced by the time that LC data is available, then the resulting theoretical uncertainty in $\hat{g}_{hcc}$ would dominate the uncertainty in the value of Δ_b extracted from Eq. 5.1. In contrast, the theoretical uncertainty in the $ht\bar{t}$ coupling is very small due to the precision in the top quark mass measurement. As discussed in Sec. 4.1, the coupling g_{htt} can be measured directly from the $e^+e^- \to t\bar{t}h$ cross section; however, this requires LC running at a higher energy, *e.g.*, $\sqrt{s} = 800$ GeV.

The LC measurements of h decay properties are sensitive to the squares of the Higgs couplings g^2_{hff} through the h partial widths; therefore the signs of the normalized couplings $\hat{g}_{hff}$ in Eq. 5.1 are not measured directly in the corresponding BRs. This leads to a potential four-fold ambiguity in the extraction of $|\Delta_b|$. However, LC measurements of $h \to gg$ and $h \to \gamma\gamma$ are sensitive to the relative signs of the Higgs couplings to the particles running in the loops; for example, flipping the sign of g_{htt} while leaving that of g_{hWW} fixed leads to a large deviation in the $h\gamma\gamma$ coupling from its SM value, while the hgg coupling is sensitive to the relative sign of g_{htt} and g_{hbb} (assuming that SUSY loops are not important). Near the decoupling limit, the radiative corrections to the CP-even Higgs mixing angle α are not so large as to change the sign of $\tan\alpha$ from its tree-level negative value, and $|\Delta_\tau| < |\Delta_b| < 1$. In this case the signs of

g_{hff} are the same as in the SM, so all the $\hat{g}_{hff}$ in Eq. 5.1 are positive.

In the discussion above, we have assumed that h is SM-like, which is appropriate once m_A is sufficiently above $m_h^{\rm max}$ (in practice, $m_A \gtrsim 150$ GeV is usually sufficient). For values of $m_A \lesssim m_h^{\rm max}$ and $\tan\beta \gg 1$, it is H which has SM-like couplings to vector boson pairs (*i.e.*, the roles of h and H are interchanged). However, a separate analysis is not required since we also have [see Eq. 2.26]

$$\frac{\hat{g}_{Hbb} - \hat{g}_{H\tau\tau}}{\hat{g}_{Htt} - \hat{g}_{Hbb}} \simeq \frac{\hat{g}_{Hbb} - \hat{g}_{H\tau\tau}}{\hat{g}_{Hcc} - \hat{g}_{Hbb}} \simeq \Delta_b \,. \tag{5.2}$$

The extraction of the normalized couplings $\hat{g}_{Hff}$ follows the same procedure as outlined above.

The upper two panels of Fig. 8 show the fractional error in the determination of Δ_b from measurements of the Higgs couplings to $b\bar{b}$, $\tau^+\tau^-$ and $t\bar{t}$, for the benchmark large μ and A_t scenario (see Table 1), in which Δ_b is quite sizable. The error in Δ_b is calculated using the fractional uncertainties in the Higgs couplings given in Table 3. In the two upper panels of Fig. 8, in the region outside of the dot-dashed contours [and also within the smaller closed dot-dashed circles], the error on Δ_b is larger than Δ_b itself, and no meaningful value for Δ_b can be obtained. Three other contour lines are shown corresponding to a fractional uncertainty in Δ_b of 50% [dotted], 10% [dashed] and 5% [solid]. Within the region bracketed only by solid contours, the relative error on Δ_b is less than 5%. There is an approximate (distorted reflection) symmetry in these contours about $m_A = m_h^{\rm max} = 119$ GeV. This corresponds to the interchange of roles between h and H at large $\tan\beta$ as noted above. Note also the convergence of the contours at $\tan\beta \sim 41$ (left panels) and $\tan\beta \sim 33$ (right panels) corresponding to the $\tan\beta$ values at which the m_A-independent decoupling occurs.

For positive μ (the upper left panel of Fig. 8), Δ_b can only be distinguished from zero at the 2σ level (*i.e.*, a 50% measurement) for moderate to large $\tan\beta$ and $m_A \lesssim 160$ GeV. For such low values of m_A, the heavy Higgs bosons will be directly observed at the LC. In contrast, for negative μ (the upper right panel of Fig. 8; note the change in the horizontal scale), Δ_b can be determined with 10% accuracy even for m_A as large as 500 GeV for large $\tan\beta$. This significant difference in sensitivity to Δ_b between the positive and negative μ cases is a combination of two effects. First, for negative μ, the bottom-squark–gluino and top-squark–Higgsino contributions to Δ_b enter with the same (negative) sign, while for positive μ they enter with opposite signs (see Eq. 2.10). Thus for fixed values of $|A_t|$ and $|\mu|$ (with $A_t\mu < 0$), $|\Delta_b|$ is larger for negative μ than for positive μ. Second, Δ_b enters the b quark Yukawa coupling non-linearly as $1/(1+\Delta_b)$, so that $\Delta_b < 0$ has a more pronounced effect.

The upper right panels of Figs. 1 and 2 demonstrate that $\Gamma(c) \propto g_{hcc}^2$ is very close to its SM value once $m_A \gtrsim 150$ GeV and $\tan\beta \gtrsim 5$. In this region of parameter space, $|\cos(\beta-\alpha)| \ll 1$ and

$$\hat{g}_{hcc} = \hat{g}_{htt} \simeq 1 + \cot\beta\cos(\beta-\alpha) + \mathcal{O}\left(\cos^2(\beta-\alpha)\right) \simeq 1 \,. \tag{5.3}$$

Thus a value of Δ_b can be extracted by taking $\hat{g}_{hcc} = \hat{g}_{htt} = 1$ in Eq. 5.1. To the extent that this is a good approximation, there is no sensitivity in the value of Δ_b to the theoretical uncertainty in the charm or top

quark Yukawa couplings. Likewise, for $m_A \lesssim m_h^{\rm max}$ and $\tan\beta \gg 1$, $\sin(\beta-\alpha)$ is close to zero so that

$$\hat{g}_{Hcc} = \hat{g}_{Htt} \simeq 1 - \cot\beta \sin(\beta-\alpha) + \mathcal{O}\left(\sin^2(\beta-\alpha)\right) \simeq 1\,, \tag{5.4}$$

and Δ_b can be extracted by taking $\hat{g}_{Hcc} = \hat{g}_{Htt} = 1$ in Eq. 5.2. Results are shown in the lower two panels of Fig. 8. With the assumption that the Higgs coupling to $t\bar{t}$ is given by its SM value, the precision in Δ_b is improved somewhat, especially for large values of $\tan\beta$ and m_A and $\mu < 0$ [the lower right panel of Fig. 8]. Note that in the region of the m_A—$\tan\beta$ plane in which $\cos(\beta-\alpha)$ takes on some intermediate value between zero and one, neither Eq. 5.3 nor Eq. 5.4 is a good approximation, and the results in the lower two panels of Fig. 8 are not reliable.

6 Conclusions

There are significant regions of MSSM parameter space where the Tevatron or LHC can discover a light Higgs boson which is indistinguishable from the SM Higgs boson using only hadron collider measurements. Additional Higgs bosons may be observed, but further measurements will be necessary to constrain the underlying Higgs sector. Also, there is a region of MSSM parameter space for moderate $\tan\beta$ and moderate to large m_A where only a single light Higgs boson with SM-like couplings would be observed in experiments at the Tevatron, the LHC, and a $\sqrt{s} = 350$ or 500 GeV e^+e^- linear collider. In this case, precision measurements of the properties of the light Higgs boson at the LC can be used to distinguish between the SM and MSSM, and further to extract or constrain the model parameters. At the LC, the production cross sections and the most important branching ratios of a light SM-like Higgs boson can be measured with precisions between 2 and 15%. We have examined how these measurements can be used to distinguish an MSSM Higgs boson from the SM Higgs boson. We have also demonstrated the extraction of the important SUSY quantity Δ_b that parameterizes the SUSY radiative corrections to the relation between the b quark mass and its Yukawa coupling.

In general, the couplings of the lightest CP-even MSSM Higgs boson h to pairs of SM particles approach their SM values in the decoupling limit of large m_A. Thus, the deviation of h partial widths from their SM values goes to zero in the limit of large m_A, except for the loop-induced couplings of h to photon or gluon pairs, which approach their SM values in the limit that both m_A and the SUSY masses are taken large simultaneously. As one moves away from the decoupling limit, the radiative corrections to the CP-even Higgs mixing angle α, the Yukawa vertex corrections Δ_b, and contributions of SUSY particles to the loop induced hgg and $h\gamma\gamma$ couplings, all contribute to deviations of the h couplings from the corresponding SM values. The sensitivity of these couplings in the m_A—$\tan\beta$ plane for distinguishing the SM-like MSSM Higgs boson from the SM Higgs boson depends strongly on the MSSM parameters. In order to illustrate this strong dependence, we have chosen three benchmark MSSM scenarios that lead to very different behavior of the Higgs couplings.

The decoupling behavior of the h partial widths at large m_A and moderate to large $\tan\beta$ is summarized qualitatively as follows: $\delta\Gamma(W) \sim m_Z^4 \cot^2\beta/m_A^4$, $\delta\Gamma(c) \sim m_Z^2 \cot^2\beta/m_A^2$, and $\delta\Gamma(b) \sim \delta\Gamma(\tau) \sim m_Z^2/m_A^2$. Moreover, there is a contribution to $\delta\Gamma(b)$ proportional to Δ_b [see Eq. 3.6], which is enhanced at large $\tan\beta$ and can further slow the approach to decoupling. Thus we expect that $\Gamma(W)$ will decouple very quickly with increasing m_A (so that $\delta\mathrm{BR}(W) \simeq \delta\Gamma_{\mathrm{tot}}$ over most of the parameter space), $\Gamma(c)$ will decouple more slowly at low $\tan\beta$ but quickly at large $\tan\beta$, and $\Gamma(b)$ and $\Gamma(\tau)$ will decouple quite slowly, at all values of $\tan\beta$. This expected behavior is borne out in the no-mixing and maximal-mixing scenarios. In the large μ and A_t scenarios the decoupling behavior of these partial widths is more complicated, because the radiative corrections to the CP-even Higgs mixing angle α are quite significant in some regions of the m_A—$\tan\beta$ plane. For some (large) values of $\tan\beta$, $\cos(\beta-\alpha)$ is driven to zero by the radiative corrections to α, leading to "m_A-independent decoupling". In particular, $\Gamma(b)$ and $\Gamma(\tau)$ attain their SM values at much lower values of m_A than would be expected from the tree-level decoupling behavior.

The m_A-independent decoupling is not an exclusive feature of the specific large values of μ and A_t chosen in our benchmark scenarios. Additional sets of MSSM parameters that exhibit m_A-independent decoupling can be found by scaling μ, A_t, $M_{\tilde{g}}$ and M_S by a common factor; in this case the value of $\tan\beta$ at which the m_A-independent decoupling occurs varies primarily due to the $\log(M_S^2/m_t^2)$ dependence of $\delta\mathcal{M}_{ij}^2$ [see Eq. 2.4]. In particular, we have found sets of MSSM parameters with relatively small M_S that exhibit m_A-independent decoupling even for $\tan\beta$ less than 10, within the parameter region in which the heavy MSSM Higgs bosons would be missed at the LHC. In this case, due to the relatively low value of M_S, deviations from the SM Higgs couplings may be observable in $h \to gg$ or $h \to \gamma\gamma$ due to top-squark and bottom-squark loop contributions.

In the case of the loop-induced Higgs couplings to gluon or photon pairs, deviations from the SM widths can occur due to SUSY loop contributions even in the limit of very large m_A. These SUSY loops decouple at large SUSY particle masses, but the decoupling can occur more slowly if X_t is large (as in the maximal-mixing scenario), resulting in several percent deviations of $\Gamma(g)$ from its SM value even for TeV mass squarks.

Because $\Gamma(b)$ dominates the total width of a 120 GeV SM-like Higgs boson over most of the MSSM parameter space, a change in $\Gamma(b)$ causes a corresponding change in Γ_{tot}, so that the resulting change in $\mathrm{BR}(b)$ is relatively small. In contrast, branching ratios for rarer Higgs decays such as $\mathrm{BR}(W)$ and $\mathrm{BR}(g)$ are sensitive both to changes in $\Gamma(W)$ and $\Gamma(g)$, respectively, and to changes in Γ_{tot}. Thus, although $\mathrm{BR}(b)$ will be the best-measured BR and that $\Gamma(b)$ typically deviates significantly from its SM value, $\mathrm{BR}(W)$ and $\mathrm{BR}(g)$ will in general be more sensitive to deviations from the SM than $\mathrm{BR}(b)$, making their high-precision measurements a priority.

To demonstrate how LC measurements of Higgs properties can be used to distinguish a SM-like MSSM Higgs boson from the SM Higgs boson, we studied the expected uncertainties in the branching ratios

of a 120 GeV SM Higgs boson to $b\bar{b}$, WW^* and gg, and performed a χ^2 analysis using the anticipated uncertainties in the squared couplings of the SM Higgs boson to $b\bar{b}$, $\tau^+\tau^-$ and gg. In particular, we draw the following conclusions for our three benchmark scenarios from the χ^2 analysis (a somewhat lower reach in m_A is obtained using the analysis of individual BR measurements):

- In the no-mixing and maximal-mixing scenarios, the MSSM Higgs boson can be distinguished from the SM Higgs boson at the 95% confidence level for $m_A \lesssim 600$ and 650 GeV, respectively, for $\tan\beta \gtrsim 5$. These limits become slightly lower for values of $\tan\beta \lesssim 5$.

- In the large μ and A_t scenario, there are regions of parameter space at large $\tan\beta$ in which the MSSM Higgs boson cannot be distinguished from the SM Higgs boson using BR and cross section measurements for any value of m_A. For $\tan\beta \lesssim 20$, the MSSM Higgs boson can be distinguished from the SM Higgs boson at the 95% confidence level for $m_A \lesssim 450$ GeV.

The precise reach in m_A in the maximal-mixing scenario should be viewed liberally, since the SM-like Higgs boson mass can reach values near 130 GeV, and some of the coupling and BR measurements used in this study have poorer precision for $m_h > 120$ GeV.

Finally, we have shown that when Δ_b is sufficiently large, information on Δ_b can be obtained from the measurements of the couplings g_{hbb}, $g_{h\tau\tau}$ and g_{htt} [or g_{hcc}] unless the MSSM parameters are such that m_A-independent decoupling occurs. The precision achievable in this measurement depends on the size and sign of Δ_b; these depend in part on the signs of $\mu M_{\tilde{g}}$ and μA_t. Combining precision measurements in the Higgs sector, such as those leading to the determination of Δ_b, with direct measurements of the SUSY spectrum will be of great value in deciphering the underlying supersymmetric structure of the theory.

Acknowledgments

We thank the organizers of the 5th International Linear Collider Workshop (LCWS 2000) at Fermilab, where portions of this work were presented. We are also grateful to S. Dawson, D. Rainwater, M. Schmitt, M. Spira and especially C. Wagner for useful comments and discussions. H.E.H. and H.E.L. thank the Aspen Center for Physics for its hospitality while this work was being completed. Fermilab is operated by Universities Research Association Inc. under contract no. DE-AC02-76CH03000 with the U.S. Department of Energy. H.E.H. is supported in part by the U.S. Department of Energy. S.M. is supported by the Department of Energy and by the Davis Institute for High Energy Physics.

References

[1] H. E. Haber and Y. Nir, Nucl. Phys. **B335**, 363 (1990); H. E. Haber, in *Physics From the Planck Scale to the Electroweak Scale*, Proceedings of the US–Polish Workshop, Warsaw, Poland, September 21–24, 1994, edited by P. Nath, T. Taylor, and S. Pokorski (World Scientific, Singapore, 1995) pp. 49–63 [hep-ph/9501320]; J.F. Gunion and H.E. Haber, in preparation.

[2] M. Carena, J. S. Conway, H. E. Haber and J. D. Hobbs, et al., Report of the Tevatron Higgs Working Group, hep-ph/0010338.

[3] K. Lassila-Perini, ETH Dissertation thesis No. 12961 (1998); ATLAS collaboration Technical Design Report, available at `http://atlasinfo.cern.ch/Atlas/GROUPS/PHYSICS/TDR/access.html`.

[4] ALEPH, DELPHI, L3 and OPAL Collaborations and the LEP Higgs Working Group, LHWG Note 2001-2, ALEPH 2001-032 CONF 2001-024, DELPHI 2001-032 CONF 473, L3 Note 2656, OPAL Technical Note TN682, prepared for the Winter 2001 conferences (26 March 2001).

[5] F. Gianotti on behalf of the ATLAS collaboration (preliminary result), private communication.

[6] P. García-Abia, W. Lohmann and A. Raspereza, in *Physics and experiments with future linear e^+e^- colliders*, Proceedings of the 5th International Linear Collider Workshop, Batavia, IL, USA, 2000, edited by A. Para and H. E. Fisk (American Institute of Physics, New York, 2001), pp. 218–221.

[7] M. Battaglia and K. Desch, in *Physics and experiments with future linear e^+e^- colliders*, Proceedings of the 5th International Linear Collider Workshop, Batavia, IL, USA, 2000, edited by A. Para and H.E. Fisk (American Institute of Physics, New York, 2001), pp. 163–182 [hep-ph/0101165].

[8] M. Battaglia, in Proceedings of the *Worldwide Study on Physics and Experiments with Future e^+e^- Linear Colliders*, edited by E. Fernandez and A. Pacheco, UAB, Barcelona, 2000, vol. I, p. 163 [hep-ph/9910271].

[9] J. F. Gunion and P. C. Martin, Phys. Rev. Lett. **78**, 4541 (1997); and in *New Directions for High Energy Physics*, Proceedings of the 1996 DPF/DPB Summer Study in High Energy Physics, Snowmass '96, edited by D.G. Cassel, L.T. Gennari and R.H. Siemann (Stanford Linear Accelerator Center Publications, Stanford, CA, 1997) pp. 637–641 [hep-ph/9610417].

[10] M. Sachwitz, H. J. Schreiber and S. Shichanin, hep-ph/9706338; E. Boos, V. Ilyin, A. Pukhov, M. Sachwitz and H. J. Schreiber, Eur. Phys. J. direct **C5**, 1 (2000).

[11] R. Van Kooten, talk given at Berkeley 2000: Workshop to Study Physics and Detectors of Future e^+e^- Colliders, LBL, Berkeley CA, 30 March 2000, slides available at `http://needmore.physics.indiana.edu/~rickv/nlc/talks/Berkeley_2000.html`.

[12] J. Brau, C. Potter and M. Iwasaki, talk presented by J. Brau at the Workshop on Physics and Detectors for Future e^+e^- Linear Colliders, Johns Hopkins University, Baltimore, 19–21 March 2001.

[13] E. Boos, J. C. Brient, D. W. Reid, H. J. Schreiber and R. Shanidze, Eur. Phys. J. **C19**, 455 (2001).

[14] J. Kamoshita, Y. Okada and M. Tanaka, Phys. Lett. **B391**, 124 (1997); S. Kiyoura and Y. Okada, in *Physics and experiments with future linear e^+e^- colliders*, Proceedings of the 5th International Linear Collider Workshop, Batavia, IL, USA, 2000, edited by A. Para and H.E. Fisk (American Institute of Physics, New York, 2001), pp. 284–287 [hep-ph/0101172].

[15] K. S. Babu and C. Kolda, Phys. Lett. **B451**, 77 (1999).

[16] J. Guasch, W. Hollik and S. Peñaranda, Phys. Lett. **B515**, 367 (2001).

[17] H. E. Logan, in *Physics and experiments with future linear e^+e^- colliders*, Proceedings of the 5th International Linear Collider Workshop, Batavia, IL, USA, 2000, edited by A. Para and H.E. Fisk (American Institute of Physics, New York, 2001), pp. 271–274 [hep-ph/0012202]; S. Mrenna, talk given at the 5th International Linear Collider Workshop, Fermilab, 24–28 October 2000, slides available at `http://conferences.fnal.gov/lcws2000/web/P1_Mrenna/`.

[18] Y. Okada, M. Yamaguchi and T. Yanagida, Prog. Theor. Phys. **85**, 1 (1991); J. Ellis, G. Ridolfi and F. Zwirner, Phys. Lett. **B257**, 83 (1991).

[19] S. P. Li and M. Sher, Phys. Lett. **B140**, 339 (1984); R. Barbieri and M. Frigeni, Phys. Lett. **B258**, 395 (1991); M. Drees and M. M. Nojiri, Phys. Rev. **D45**, 2482 (1992); J. A. Casas, J. R. Espinosa, M. Quiros and A. Riotto, Nucl. Phys. **B436**, 3 (1995) [E: **B439**, 466 (1995)].

[20] J. Ellis, G. Ridolfi and F. Zwirner, Phys. Lett. **B262**, 477 (1991); A. Brignole, J. Ellis, G. Ridolfi and F. Zwirner, Phys. Lett. **B271**, 123 (1991) [E: **B273**, 550 (1991)].

[21] R.-J. Zhang, Phys. Lett. **B447**, 89 (1999); J. R. Espinosa and R.-J. Zhang, JHEP **0003**, 026 (2000); J. R. Espinosa and R.-J. Zhang, Nucl. Phys. B **586**, 3 (2000).

[22] J. F. Gunion and A. Turski, Phys. Rev. **D39**, 2701 (1989); Phys. Rev. **D40**, 2333 (1989).

[23] H. E. Haber and R. Hempfling, Phys. Rev. Lett. **66**, 1815 (1991).

[24] A. Brignole, Phys. Lett. **B277**, 313 (1992).

[25] M. S. Berger, Phys. Rev. **D41**, 225 (1990); A. Brignole, Phys. Lett. **B281**, 284 (1992); M. A. Díaz and H. E. Haber, Phys. Rev. **D45**, 4246 (1992); **D46**, 3086 (1992).

[26] P. H. Chankowski, S. Pokorski and J. Rosiek, Phys. Lett. **B274**, 191 (1992); Nucl. Phys. **B423**, 437 (1994); A. Yamada, Phys. Lett. **B263**, 233 (1991); Z. Phys. **C61**, 247 (1994); A. Dabelstein, Z. Phys. **C67**, 495 (1995).

[27] D. M. Pierce, J. A. Bagger, K. Matchev and R.-J. Zhang, Nucl. Phys. **B491**, 3 (1997).

[28] R. Hempfling and A.H. Hoang, Phys. Lett. **B331**, 99 (1994).

[29] H. E. Haber, R. Hempfling and A. H. Hoang, Z. Phys. C **75**, 539 (1997).

[30] S. Heinemeyer, W. Hollik and G. Weiglein, Phys. Rev. **D58**, 091701 (1998); Phys. Lett. **B440**, 296 (1998); Eur. Phys. J. **C9**, 343 (1999).

[31] M. Carena, S. Heinemeyer, C. E. M. Wagner and G. Weiglein, hep-ph/9912223.

[32] R. Barbieri, M. Frigeni and F. Caravaglios, Phys. Lett. **B258**, 167 (1991); Y. Okada, M. Yamaguchi and T. Yanagida, Phys. Lett. **B262**, 54 (1991); D. M. Pierce, A. Papadopoulos and S. Johnson, Phys. Rev. Lett. **68**, 3678 (1992); K. Sasaki, M. Carena and C. E. M. Wagner, Nucl. Phys. **B381**, 66 (1992); R. Hempfling, in *Phenomenological Aspects of Supersymmetry*, edited by W. Hollik, R. Rückl and J. Wess (Springer-Verlag, Berlin, 1992) p. 260–279; J. Kodaira, Y. Yasui and K. Sasaki, Phys. Rev. **D50**, 7035 (1994).

[33] J. R. Espinosa and M. Quiros, Phys. Lett. **B266**, 389 (1991).

[34] H. E. Haber and R. Hempfling, Phys. Rev. **D48**, 4280 (1993).

[35] M. Carena, J. R. Espinosa, M. Quiros and C. E. M. Wagner, Phys. Lett. **B355**, 209 (1995); M. Carena, M. Quiros and C. E. M. Wagner, Nucl. Phys. **B461**, 407 (1996).

[36] M. Carena, H. E. Haber, S. Heinemeyer, W. Hollik, C. E. M. Wagner and G. Weiglein, Nucl. Phys. **B580**, 29 (2000).

[37] J. R. Espinosa and I. Navarro, Nucl. Phys. **B615**, 82 (2001).

[38] G. Degrassi, P. Slavich and F. Zwirner, Nucl. Phys. **B611**, 403 (2001).

[39] J. A. Coarasa, R. A. Jiménez and J. Solà, Phys. Lett. **B389**, 312 (1996); R. A. Jiménez and J. Solà, Phys. Lett. **B389**, 53 (1996); A. Bartl, H. Eberl, K. Hikasa, T. Kon, W. Majerotto and Y. Yamada, Phys. Lett. **B378**, 167 (1996).

[40] L. Hall, R. Rattazzi and U. Sarid, Phys. Rev. **D50**, 7048 (1994); R. Hempfling, Phys. Rev. **D49**, 6168 (1994).

[41] M. Carena, M. Olechowski, S. Pokorski and C. E. M. Wagner, Nucl. Phys. **B426**, 269 (1994).

[42] A. Dabelstein, Nucl. Phys. **B456**, 25 (1995).

[43] M. Carena, S. Mrenna and C. E. M. Wagner, Phys. Rev. **D60**, 075010 (1999).

[44] H. E. Haber, M. J. Herrero, H. E. Logan, S. Peñaranda, S. Rigolin and D. Temes, Phys. Rev. **D63**, 055004 (2001).

[45] S. Heinemeyer, W. Hollik and G. Weiglein, Eur. Phys. J. **C16**, 139 (2000).

[46] M. Carena, J. Ellis, A. Pilaftsis and C. E. M. Wagner, Nucl. Phys. **B586**, 92 (2000);

[47] S. Y. Choi, M. Drees and J. S. Lee, Phys. Lett. **B481**, 57 (2000); S. Y. Choi and J. S. Lee, Phys. Rev. **D61**, 015003 (2000).

[48] M. Carena, S. Mrenna and C. E. M. Wagner, Phys. Rev. **D62**, 055008 (2000).

[49] D. Comelli and J. R. Espinosa, Phys. Lett. **B388**, 793 (1996); J. R. Espinosa and J. F. Gunion, Phys. Rev. Lett. **82**, 1084 (1999).

[50] M. Carena, D. Garcia, U. Nierste and C. E. M. Wagner, Phys. Lett. **B499**, 141 (2001).

[51] W. Loinaz and J. D. Wells, Phys. Lett. **B445**, 178 (1998); G. L. Kane, G. D. Kribs, S. P. Martin and J. D. Wells, Phys. Rev. **D53**, 213 (1996); H. Baer and J. D. Wells, Phys. Rev. **D57**, 4446 (1998).

[52] G. Degrassi, P. Gambino and G. F. Giudice, JHEP **0012**, 009 (2000).

[53] A. Djouadi, J. Kalinowski and M. Spira, Comput. Phys. Commun. **108**, 56 (1998).

[54] A. Djouadi, V. Driesen, W. Hollik and J. I. Illana, Eur. Phys. J. **C1**, 149 (1998); A. Djouadi, Phys. Lett. **B435**, 101 (1998).

[55] J.A. Aguilar-Saavedra *et al.* [ECFA/DESY LC Physics Working Group], *TESLA Technical Design Report, Part 3: Physics at an e^+e^- linear collider* [hep-ph/0106315].

[56] K. Desch, private communication.

[57] S. Söldner-Rembold and G. Jikia, Nucl. Instrum. Meth. **A472**, 133 (2001); M. Melles, W. J. Stirling and V. A. Khoze, Phys. Rev. **D61**, 054015 (2000).

[58] I.F. Ginzburg, M. Krawczyk and P. Osland, in *Proceedings of the 4th International Workshop on Linear Colliders*, 28 April–5 May, 1999, Sitges, Spain, p. 524 [hep-ph/9909455]; in the *2nd ECFA/DESY Study 1998-2001*, pp. 1705–1733 [hep-ph/0101208]; and in *Physics and experiments with future linear*

e^+e^- *colliders*, Proceedings of the 5th International Linear Collider Workshop, Batavia, IL, USA, 2000, edited by A. Para and H.E. Fisk (American Institute of Physics, New York, 2001), pp. 304–311 [hep-ph/0101331].

[59] K. Desch and M. Battaglia, LC-PHSM-2001-053, `http://www.desy.de/~lcnotes/`.

[60] A. Juste and G. Merino, hep-ph/9910301; H. Baer, S. Dawson and L. Reina, Phys. Rev. **D61**, 013002 (2000).

[61] D. E. Groom *et al.* [Particle Data Group Collaboration], Eur. Phys. J. **C15**, 1 (2000).

[62] M. Eidemuller and M. Jamin, Phys. Lett. **B498**, 203 (2001).

[63] A.H. Hoang, CERN-TH-2000-227 [hep-ph/0008102].

[64] H. Fusaoka and Y. Koide, Phys. Rev. **D57**, 3986 (1998);

[65] D. Becirevic, V. Lubicz and G. Martinelli, hep-ph/0107124.

[66] A. H. Hoang *et al.*, Eur. Phys. J. direct **C3**, 1 (2000) [hep-ph/0001286].

[67] S. Dawson and L. Reina, Phys. Rev. D **59**, 054012 (1999).

[68] D. Zeppenfeld, R. Kinnunen, A. Nikitenko and E. Richter-Wąs, Phys. Rev. **D62**, 013009 (2000).

[69] D. Rainwater, Phys. Lett. **B503**, 320 (2001).

[70] V. A. Mitsou, ATLAS Internal Note ATL-PHYS-2000-021.

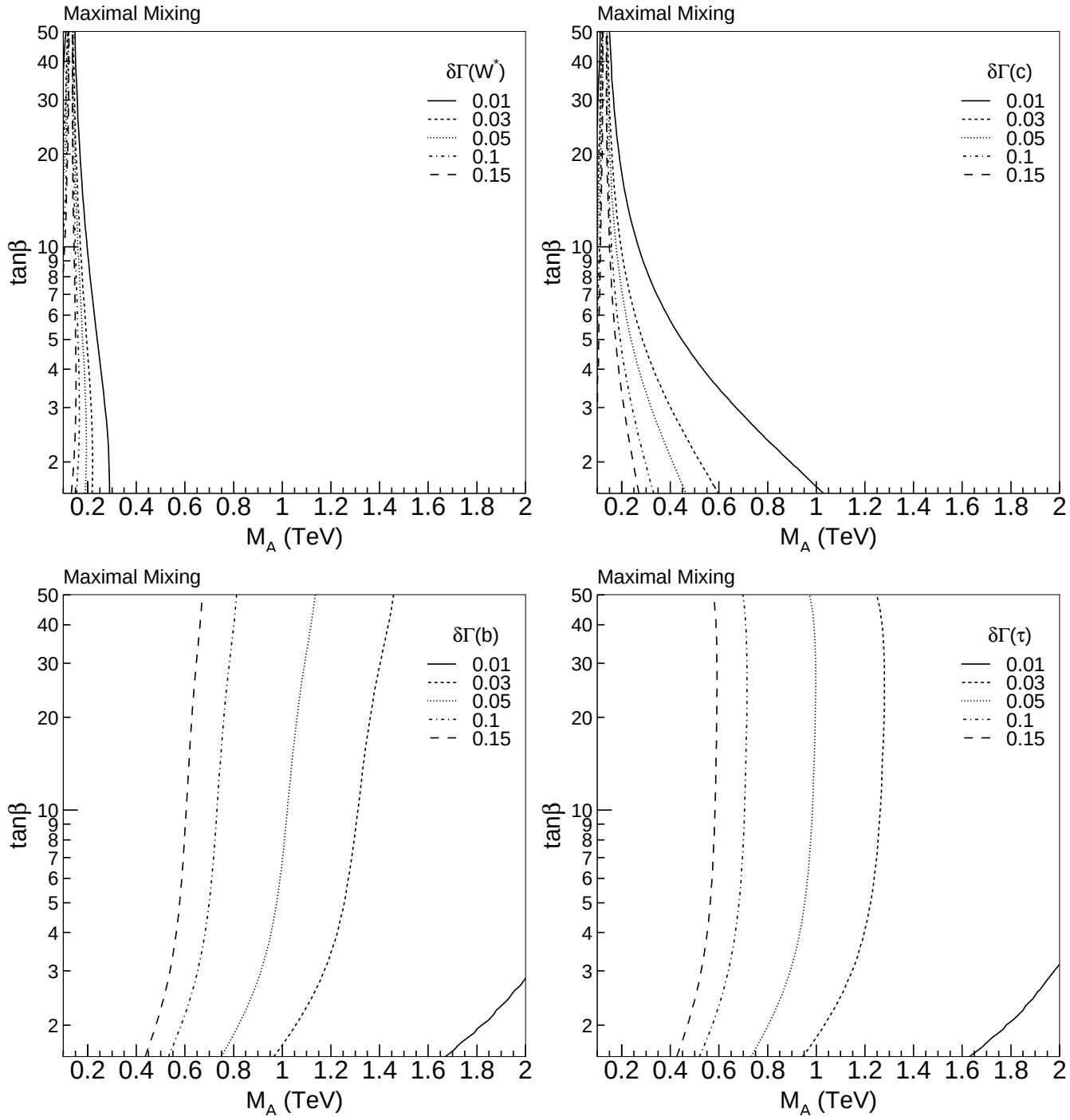

Figure 1: Deviations of Higgs partial widths from their SM values in the maximal-mixing scenario.

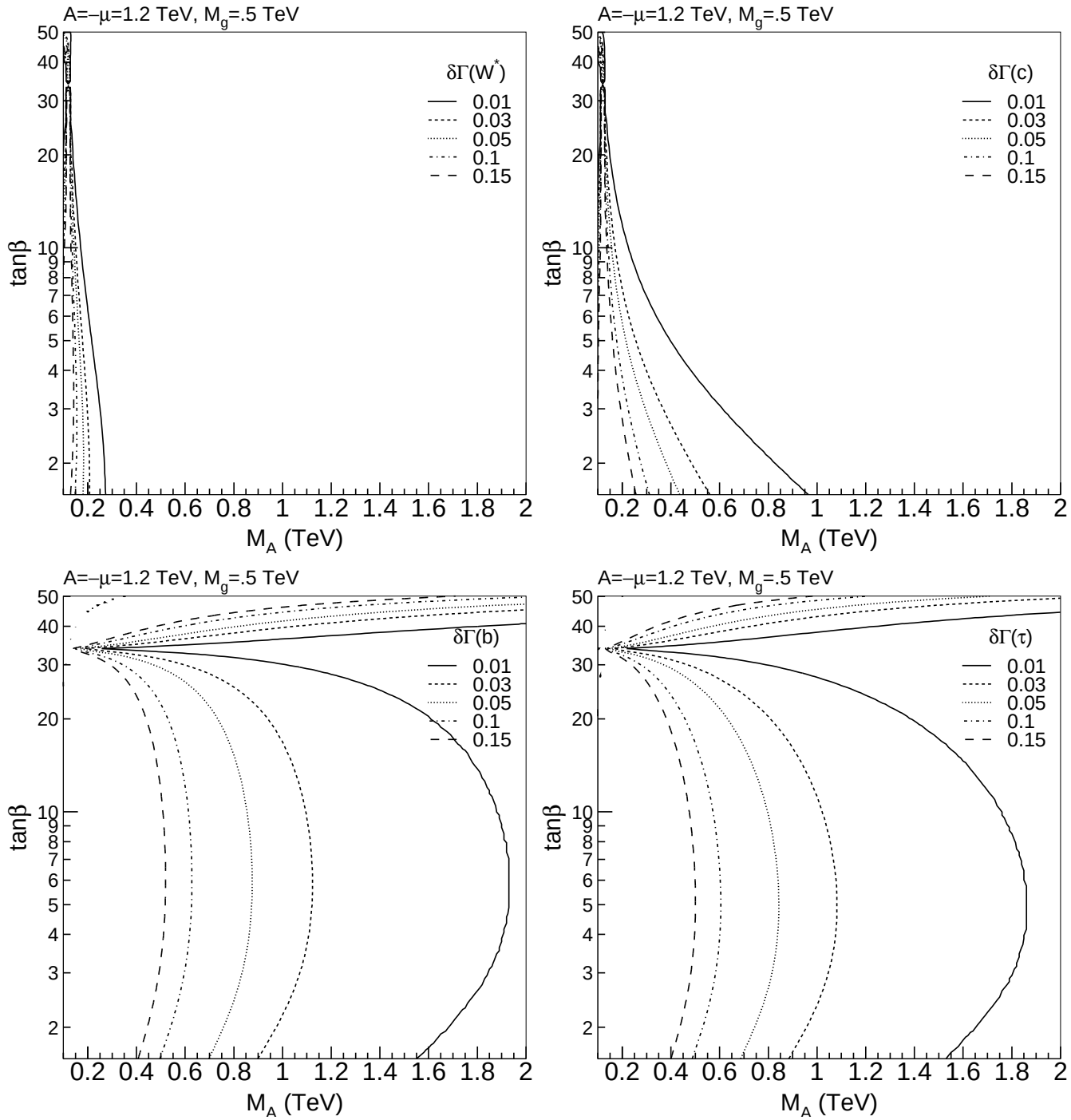

Figure 2: Deviations of Higgs partial widths from their SM values in the large μ and A_t scenario, with $A_t = -\mu = 1.2$ TeV.

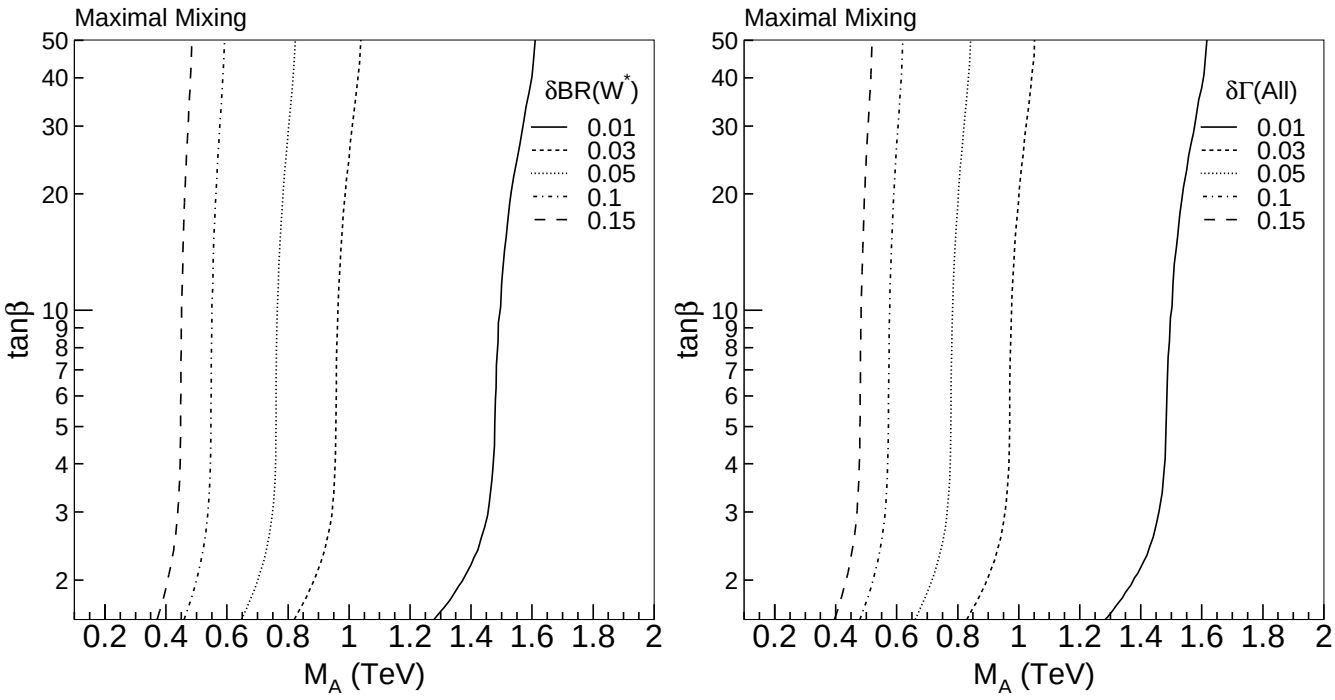

Figure 3: Deviations of BR(W) and $\Gamma_{\rm tot}$ from their SM values in the maximal-mixing scenario.

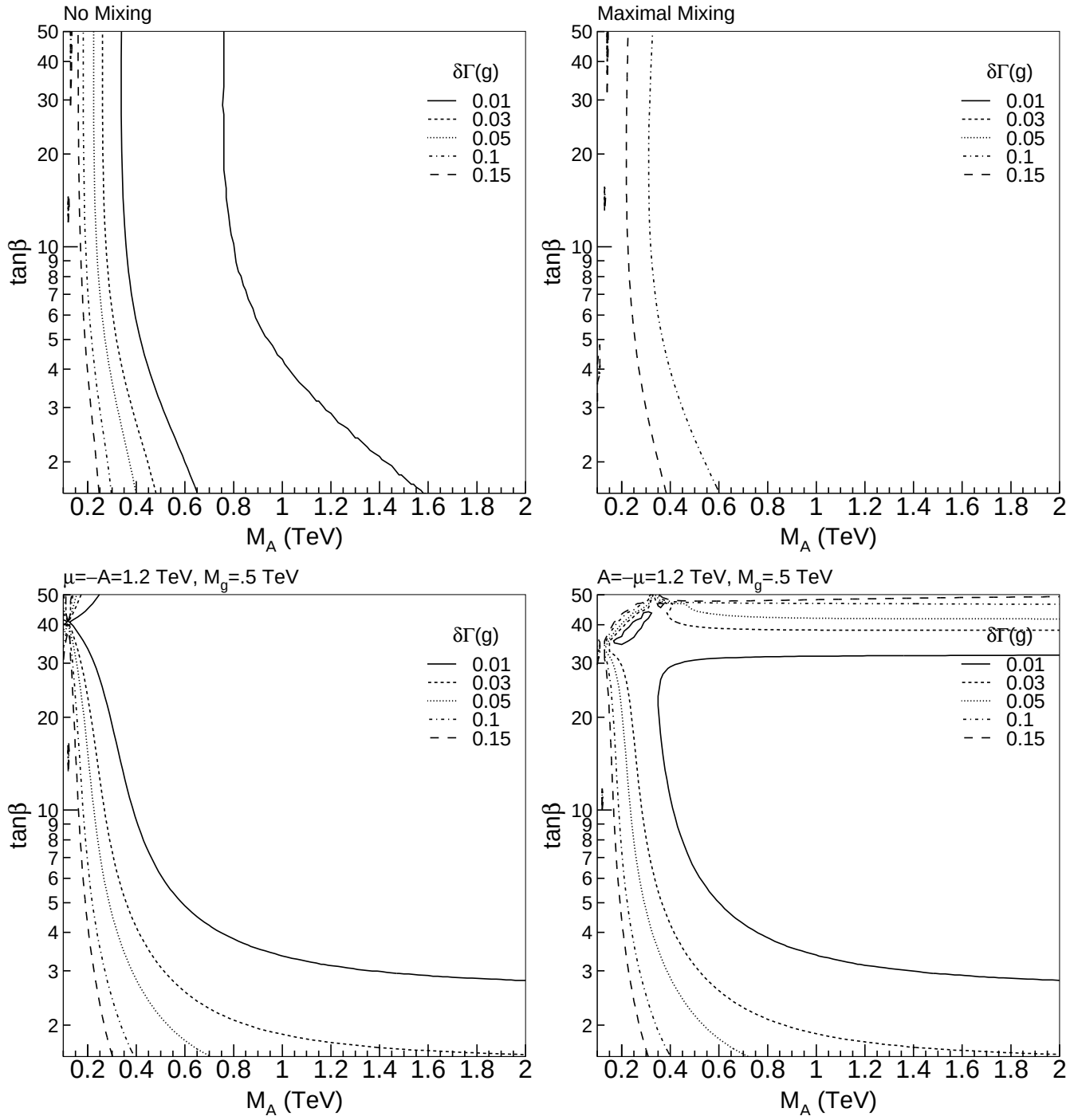

Figure 4: Deviations of the partial width $\Gamma(g)$ from its SM value in the no-mixing scenario (top left), the maximal-mixing scenario (top right), and the large μ and A_t scenario with $\mu = -A_t = 1.2$ TeV (bottom left) and $\mu = -A_t = -1.2$ TeV (bottom right). In the no-mixing scenario, $\Gamma(g)_{\rm MSSM} - \Gamma(g)_{\rm SM}$ changes sign and thus passes through zero [*i.e.*, $\delta\Gamma(g)$=0] along a contour between the two $\delta\Gamma(g) = 0.01$ contours (solid lines) exhibited in the top left panel.

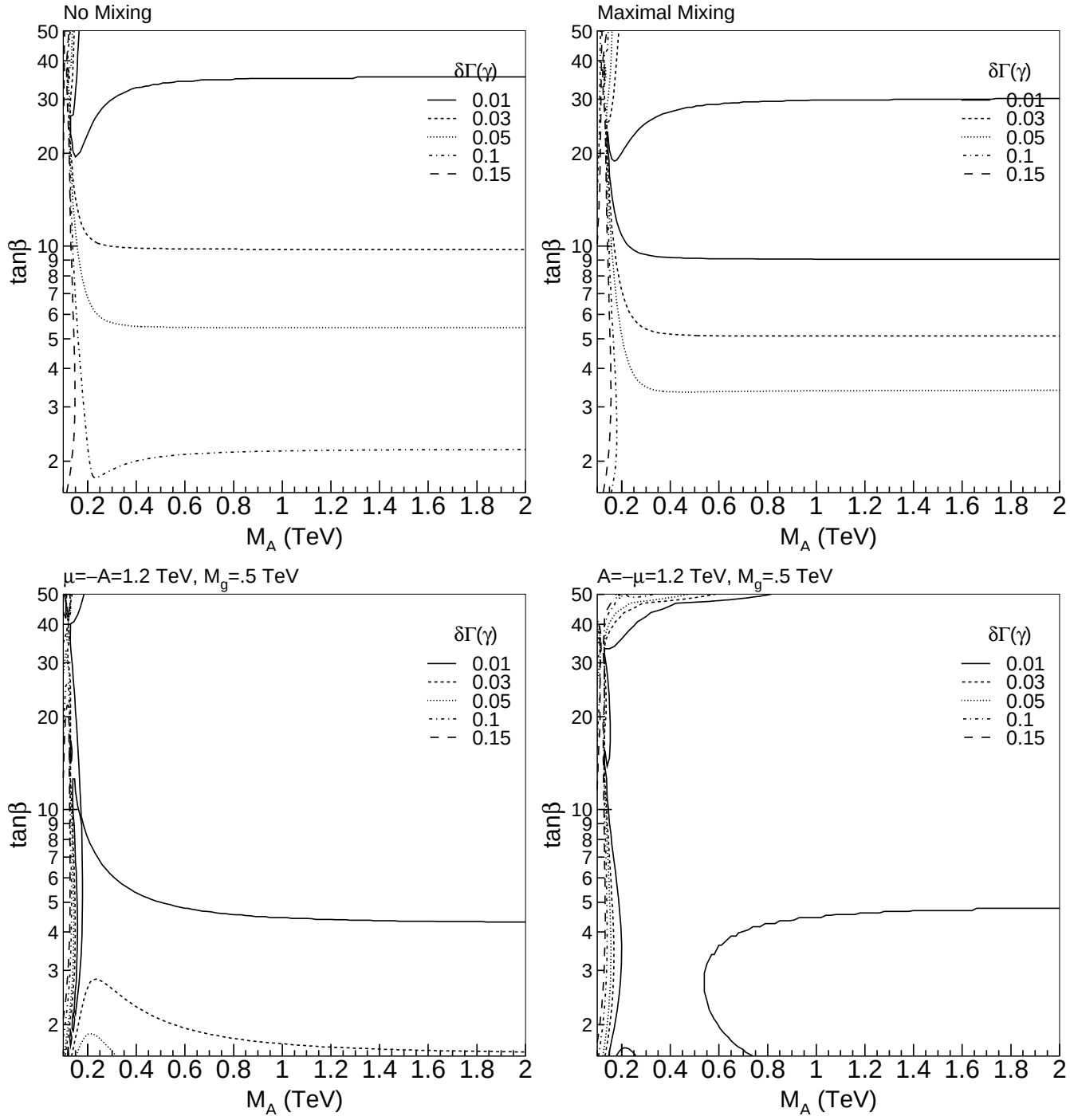

Figure 5: Deviations of the partial width $\Gamma(\gamma)$ from its SM value in the three benchmark scenarios.

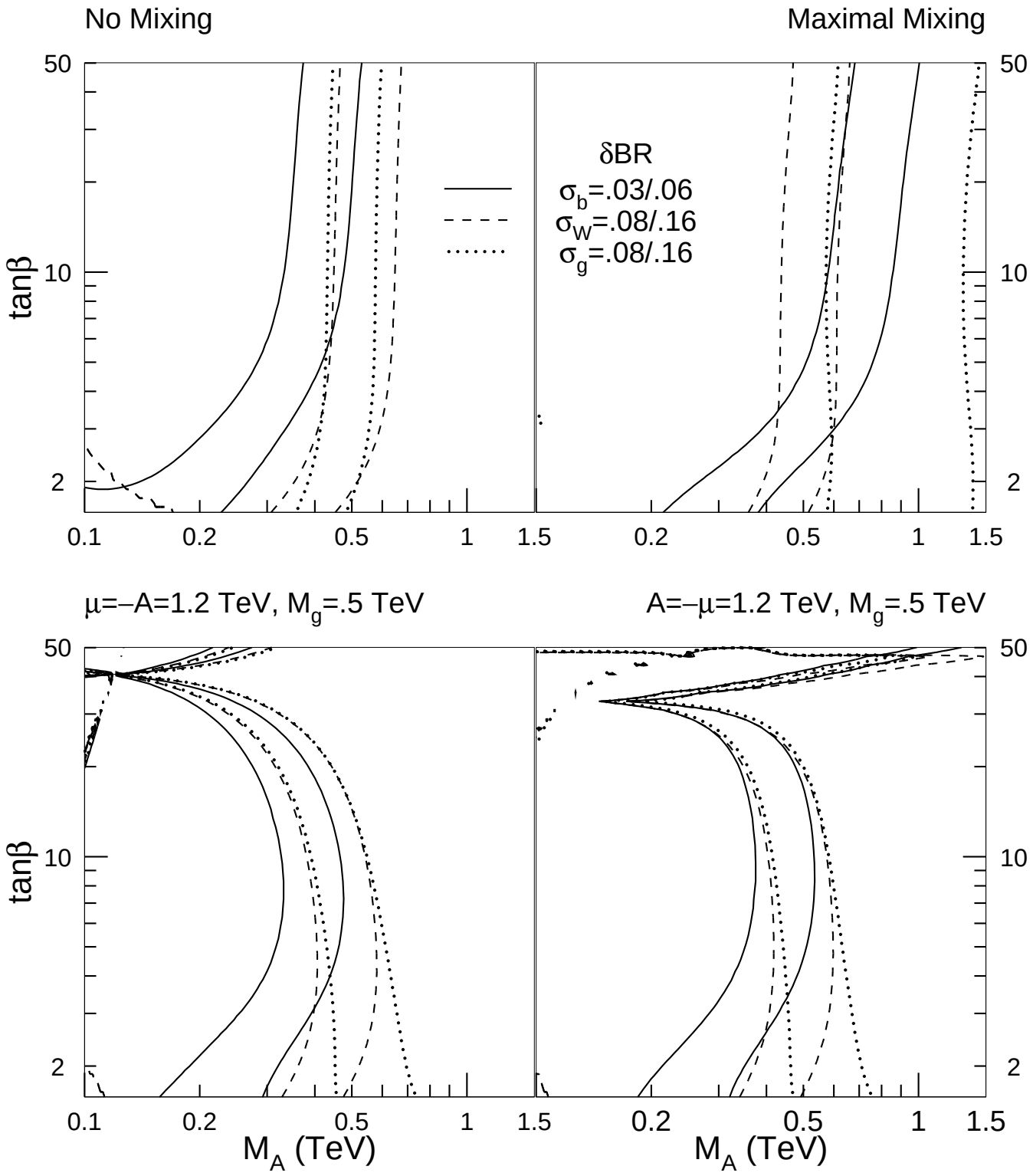

Figure 6: Contours of $\delta\mathrm{BR}(b) = 3$ and 6% (solid), $\delta\mathrm{BR}(W) = 8$ and 16% (long-dashed) and $\delta\mathrm{BR}(g) = 8$ and 16% (short-dashed) in the three benchmark scenarios.

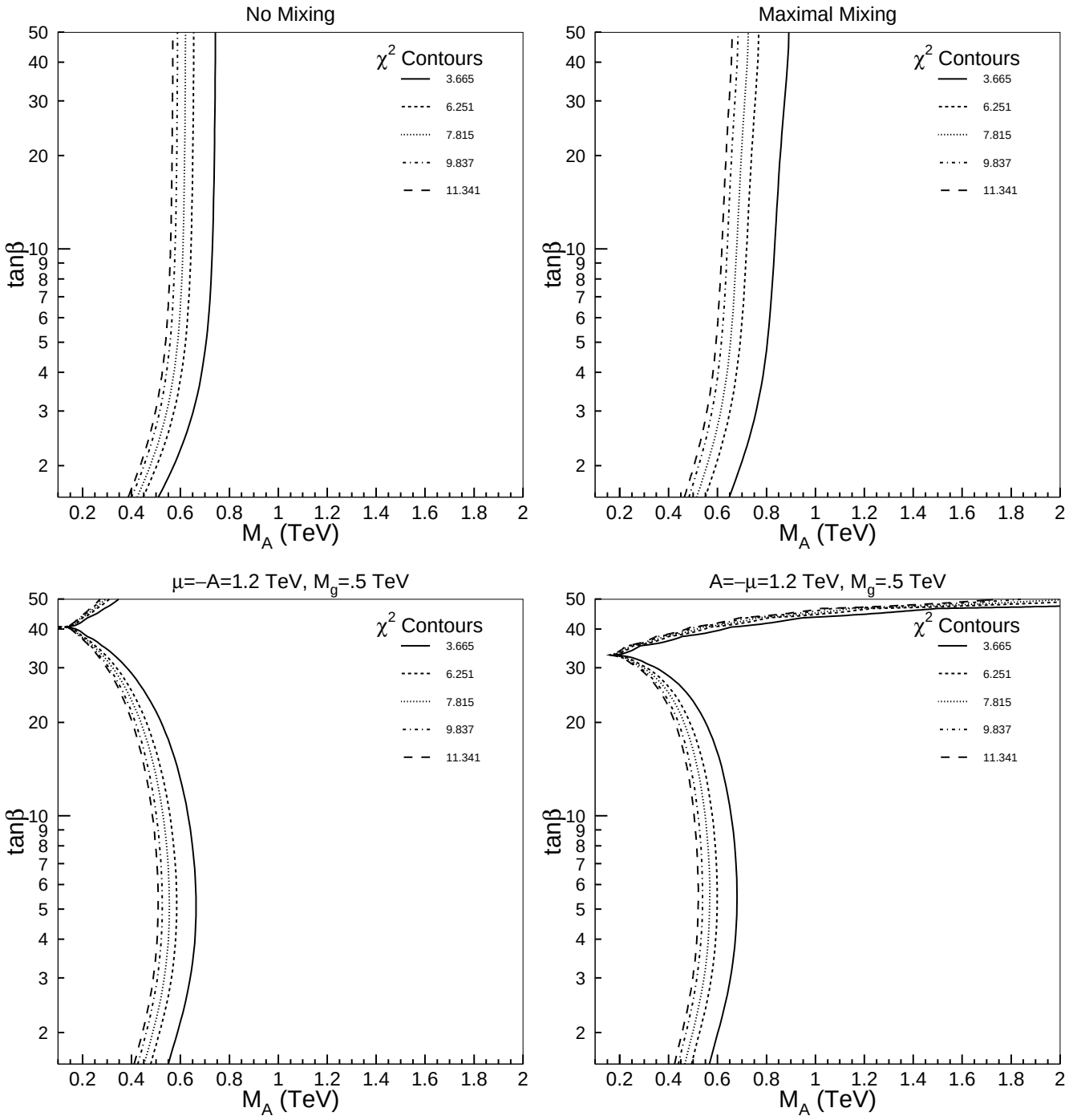

Figure 7: Contours of χ^2 for Higgs boson decay observables in the benchmark scenarios. The contours correspond to 68, 90, 95, 98 and 99% confidence levels (right to left) for the three observables g^2_{hbb}, $g^2_{h\tau\tau}$, and g^2_{hgg}.

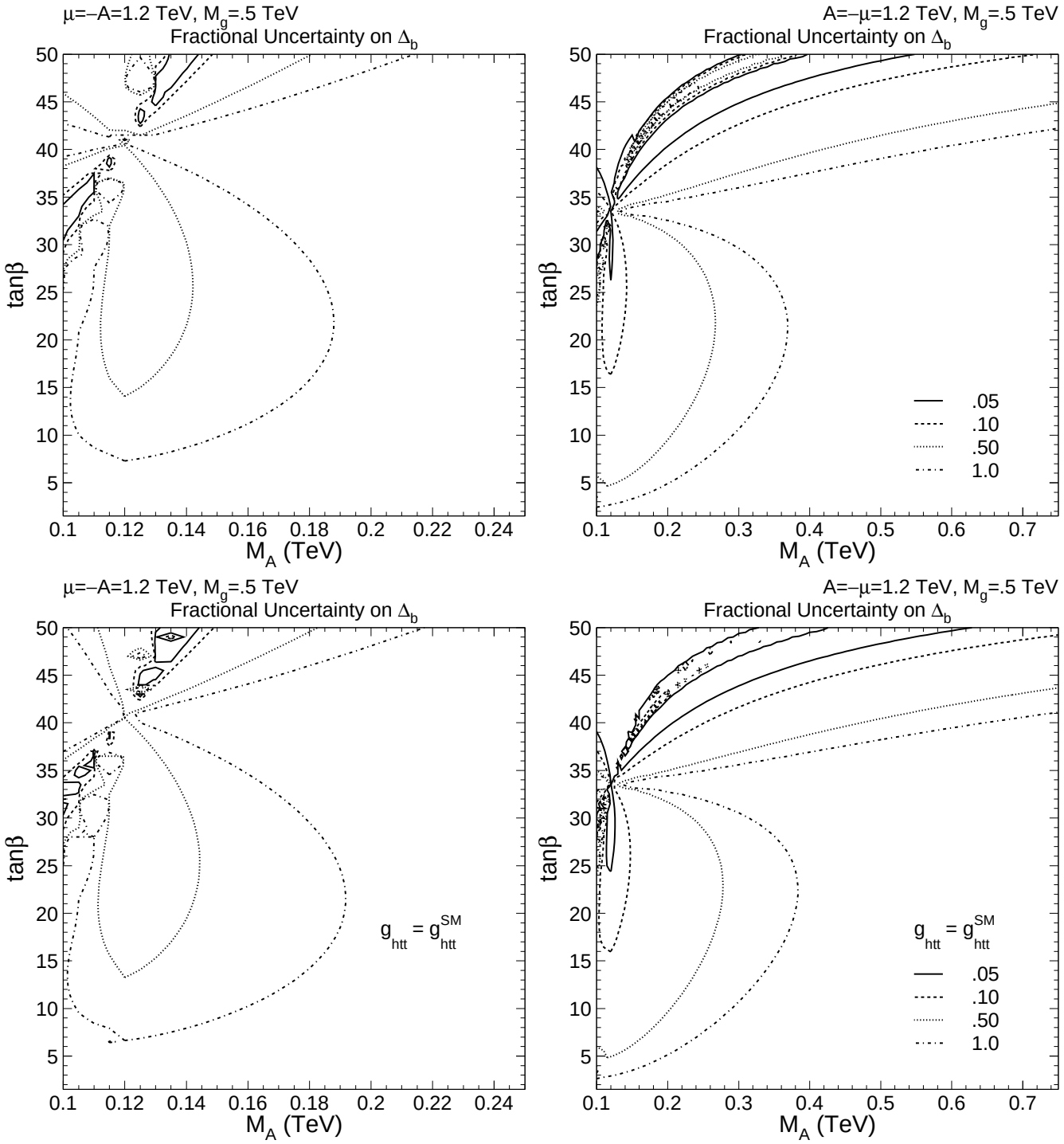

Figure 8: Contours of the fractional uncertainty in the determination of Δ_b in the large μ and A_t scenario with $\mu = -A_t = 1.2$ TeV ($\Delta_b > 0$) (left) and $\mu = -A_t = -1.2$ TeV ($\Delta_b < 0$) (right). The upper two plots use the Higgs couplings to $b\bar{b}$, $\tau^+\tau^-$ and $t\bar{t}$ as inputs while the lower two plots use only the first two couplings as input while taking the Higgs coupling to $t\bar{t}$ equal to its SM value (see Eqs. 5.3 and 5.4). In the $\mu = -A_t = 1.2$ TeV scenario (left), we plot $0.1\,\text{TeV} < m_A < 0.25\,\text{TeV}$, while in the $\mu = -A_t = -1.2$ TeV scenario (right), we plot $0.1\,\text{TeV} < m_A < 0.75\,\text{TeV}$.